NASA Contractor Report 3681

Terminal Area Automatic Navigation, Guidance, and Control Research Using the Microwave Landing System (MLS)

Part 5 - Design and Development of a Digital Integrated Automatic Landing System (DIALS) for Steep Final Approach Using Modern Control Techniques

Nesim Halyo

CONTRACT NAS1-15116
APRIL 1983

25th Anniversary
1958-1983

NASA

NASA Contractor Report 3681

Terminal Area Automatic Navigation, Guidance, and Control Research Using the Microwave Landing System (MLS)

Part 5 - Design and Development of a Digital Integrated Automatic Landing System (DIALS) for Steep Final Approach Using Modern Control Techniques

Nesim Halyo
Analytical Mechanics Associates, Inc.
Hampton, Virginia

Prepared for
Langley Research Center
under Contract NAS1-15116

National Aeronautics
and Space Administration

**Scientific and Technical
Information Branch**

1983

FOREWORD

The work described in this report was performed under Contract Number NAS1-15116 for the National Aeronautics and Space Administration (NASA), Langley Research Center (LRC), Hampton, Virginia. The work was sponsored by the Flight Control Systems Division at LRC. Mr. R. M. Hueschen was the NASA Technical Representative monitoring this contract. Dr. N. Halyo directed the technical effort at AMA.

TABLE OF CONTENTS

LIST OF FIGURES

LIST OF SYMBOLS

VARIABLE	DESCRIPTION
A	System Matrix
$a_{(\cdot)}$	Acceleration along the subscripted axis
a_{ij}	Element $[i,j]$ in the A matrix
B	Control effect matrix
b	Aircraft wing span
b_{ij}	Element $[i,j]$ in the B matrix
C_D	Aerodynamic drag coefficient
C_L	Aerodynamic lift coefficient
C_M	Aerodynamic pitch coefficient
C_T	Aerodynamic thrust coefficient
c_i	Gain in localizer capture criterion
$c_{\ell i}$	Gain in glideslope capture criterion
D	Wind disturbance effect matrix
E	Expected value
e	Tracking error vector
$\bar{e}_i$	Estimated error in the state x_i
f_{T_x}	Perturbation in thrust along the x_s direction
f_{T_y}	Perturbation in the thrust force along y_s
f_{T_z}	Perturbation in thrust along the z_s direction
f_{A_x}	Perturbation in net aerodynamic force along the x_s direction
f_{A_y}	Perturbation in the net aerodynamic force along y_s
f_{A_z}	Perturbation in net aerodynamic force along the z_s direction

LIST OF SYMBOLS (CONTINUED)

VARIABLE	DESCRIPTION
G_{ij}	Intermediate optimal feedback gain calculation
$G_{(\cdot)}$	Transfer function for gusts
H_{ij}	Optimal Feedback Gain
H_f	Altitude at touchdown
h_{ij}	Element $[i,j]$ in the D matrix
I_{xx}, I_{zz}, I_{xx}, I_{yy}	Moments of Inertia of the aircraft in the stability axes
J	Discrete-time cost function
J_c	Continuous-time cost function
j	$\sqrt{-1}$
k	Index
L	Scale of turbulence
L_{ES}	Transformation from stability axes to the earth-fixed axes
L_{SE}	Transformation from earth-fixed axes to the stability axes
$\bar{L}_{ij}$	Filtered estimate of $L_{ES}(i,j)$
ℓ_A	Perturbation in the rolling moment due to aerodynamic forces
ℓ_T	Perturbation in the rolling moment due to thrust
m	Aircraft mass
m_A	Perturbation in pitching moment due to aerodynamic forces
m_T	Perturbation in pitching moment due to thrust
N	Number of steps summed in discrete-time cost function
n_A	Perturbation in the yawing moment due to aerodynamic forces
n_T	Perturbation in the yawing moment due to thrust
P_{ij}	Discrete optimal control Riccati equation solution
P	Perturbation in the roll rate about x_s

LIST OF SYMOBLS (CONTINUED

VARIABLE	DESCRIPTION
Q	State weighting matrix
q	Pitch rate
$\bar{q}$	Dynamic pressure
R	Control weighting matrix
r	Perturbation in the yaw rate about z_s
S	Effective wing area
$S_{(\cdot)}$	Spectra for longitudinal gusts
s	Laplace operator
T_o	Sample time
t_f	Final time in cost function evaluation
U_o	Nominal inertial speed in the x_s direction
u	Perturbation in inertial speed along the x_s direction
V_a	Aircraft airspeed
v	Perturbation in the inertial speed along the stability y-axis, i.e., along y_s
W	Wind state vector
w	Inertial speed along the z_s direction
X_f	Touchdown point of aircraft on landing
$\bar{x}_e$	Estimated ground distance to GPIP
x_e, x_b, x_s	Position along the earth-fixed, body-fixed, stability x-axis, respectively
y_e, y_b, y_s	Position along the earth-fixed, body-fixed, stability y-axis, respectively
z_3	Commanded inertial sideslip angle
$z_{\ell 3}$	Commanded inertial angle of attack
z_e, z_b, z_s	Position along the earth-fixed, body-fixed, stability z-axis, respectively

LIST OF SYMBOLS (CONTINUED)

VARIABLE (GREEK)	DESCRIPTION
α	Angle of attack
β	Angle of sideslip
$\bar{\beta}_{ws}$	Estimate of the steady wind velocity
Γ	Discrete-time control effect matrix
γ_o	Glideslope angle
δe	Perturbation of elevator
δs	Perturbation of stabilizer
δT	Perturbation of thrust
δth	Perturbation of throttle
η	External disturbances
θ	Perturbation in pitch angle
ξ	Vector zero everywhere except ξ_1 which is defined in (85), White noise forcing function
π	3.14 ...
Σ	Summation
σ	Variance
ϕ	Perturbation in the roll angle, Discrete-time state transition matrix
Ω	Spatial frequency in gust model
ω_1	Gaussian white noise wind model forcing function
ω	Gaussian white noise process
$\bar{\omega}$	Temporal frequency

SUBSCRIPTS	DESCRIPTION
A	Aerodynamic related
b	Body-axis
e	Earth-axis
g	Gust related
ℓ	Longitudinal axes vector
o	Nominal value
s	Stability axis
S	Shear state
T	Thrust related
w	Component due to wind
x	Vertical perpendicular to x and y
y	Horizontal perpendicular to x and z
z	Horizontal perpendicular to x and y

PUNCTUATION	DESCRIPTION
$(\dot{})$	Derivative of quantity with respect to time
$(\hat{})$	Discrete cost function weighting matrix
$( )'$	Normalized value
$( )^T$	Transpose
∞	Infinity
$\int$	Integral

LIST OF SYMBOLS (CONTINUED)

ACRONYM	CORRESPONDING PHRASE
DIALS	Digital Integrated Automatic Landing System
GPIP	Glidepath Intercept Point
ILS	Instrument Landing System
LQG	Linear Quadratic Gaussian
MLS	Microwave Landing System
NASA	National Aeronautics and Space Administration
TCV	Terminal Configured Vehicle

I. INTRODUCTION

To meet projected aviation requirements NASA's Langley Research Center is conducting a research and development effort, the Terminal Configured Vehicle (TCV) program, to develop advanced technology for improved terminal area operational capability and safety of transport aircraft. The TCV program is aimed at developing capabilities for increased terminal area capacity, safe and accurate flight in adverse weather conditions including shear winds, noise reduction, the avoidance of wake vorticies and reduced fuel consumption. Advances in digital flight computers and modern control theory, coupled with accurate guidance information such as that provided by the Microwave Landing System can be effectively used to achieve some of these goals. The work described in this report has evolved within the TCV program framework [1], [2].

The design of the Digital Integrated Automatic Landing System (DIALS) was completed in 1980. The automatic landing system was implemented on the TCV research aircraft, a Boeing 737-100. DIALS was flight tested with successful test results by NASA's Langley Research Center at Wallops Island Center, thus demonstrating the application of modern control theory to a complex design problem. The DIALS flight tests were completed in December 1981. DIALS is the first digital automatic landing system designed with a modern control structure and methodology which has been successfully flight tested, to the author's knowledge. This report describes the design and development of the Digital Integrated Automatic Landing System prior to flight testing.

The implementation and flight results will be given in detail in a subsequent report.

DIALS uses the Microwave Landing System (MLS) which is a guidance system providing high accuracy position information in the form of azimuth, elevation, and range measurements. As the Microwave Landing System is less sensitive to weather conditions than conventional systems, automatic landing systems using the MLS can be used to reduce the congestion in terminal areas due to adverse weather conditions. Furthermore, the volumetric coverage provided by the MLS enables the use of curved flight paths and steep glideslopes in the final approach and landing phase of the flight. The guidance system consists of the DME providing range information, an azimuth antenna generally co-located with the DME antenna providing the aircraft's azimuth angle relative to the runway centerline up to ±60°, and an elevation antenna located at the glidepath intercept point but offset to the side of the runway providing the aircraft's elevation angle up to 20°. An onboard MLS receiver provides high accuracy position information that can be used for steep approaches and curved flight paths in the terminal area.

This report describes the design and development of a Digital Integrated Automatic Landing System (DIALS) for the TCV research aircraft, a B-737-100 aircraft through the use of modern control methodologies and structures. The system uses MLS position information, as well as onboard sensor measurements; the system was developed using modern digital control methodologies [3], [4], [5], [6]. The phases of the final approach and landing considered are localizer and glideslope capture and track, crab/decrab, and flare. The system captures, tracks, and flares from a steep glideslope selected by the pilot prior

to engaging the capture mode. Thus, the control system modes designed are:

1) Localizer capture
2) Steep Glideslope capture
3) Localizer track
4) Steep Glideslope track
5) Decrab
6) Flare

Two important features of the system are:

- the simultaneous capture of the localizer and glideslope when necessary, and
- the selectable steep glideslope (2.5° - 5.5° for the B-737)

Typically, the aircraft is positioned, manually or automatically, below the selected glideslope so as to intercept the localizer at a selected airspeed, as shown in Fig. 1. When the localizer or glideslope capture criteria are satisfied, the corresponding capture mode is engaged; so that depending on the initial aircraft position and attitude, the localizer and glideslope can be captured simultaneously or sequentially. As the aircraft reaches the localizer or glideslope, the corresponding track (or hold) modes are engaged. When a cross-wind component is present, the control system crabs the aircraft into the wind, followed by a decrab maneuver when the decrab altitude is reached. A flare path which depends on the glideslope selected for a given approach is generated on-line, and the aircraft is controlled about this path until touchdown.

The main considerations in the development of DIALS include:

- low overshoots of the localizer and steep glideslope under adverse wind conditions
- quick settling on the trajectory
- overall smoothness of the flight during the final approach
- accurate tracking in adverse weather conditions including gusts and shear winds

The ability to follow various steep glideslopes (selectable until glideslope capture) provides a flexibility which can increase the efficiency of terminal area operations, reduce the noise perceived on the ground, and can be used for vortex avoidance when following a large aircraft, while reducing fuel consumption during a steep final approach. Capturing the glideslope and localizer simultaneously and with quick settling times allows close-in captures, while low overshoots of the localizer under adverse wind conditions enhance the independence of close parallel runway operations. Finally, the low degradation of the MLS information accuracy in adverse weather conditions enhances performance capabilities under low visibility conditions.

The overall objective in the development of DIALS has been the direct-digital-design (using modern control methods) of an automatic landing system which controls the aircraft from the localizer and glideslope angles between 2.5° - 5.5°, nominal airspeeds between 115 - 135 knots, aircraft weights between 70,000 - 90,000 lbs, c.g. locations between .2 - .3 under adverse wind conditions and low visibility. As the control objectives during different phases of the final approach vary, the most important desirable characteristics of the control law

in the various portions of the flight are different. For example, while low overshoot characteristics are important during capture, vertical path accuracy becomes more significant in flare. A more detailed description of the desirable characteristics in the various control modes is given in Section IV. To achieve these varying objectives, it appears that some changes in the control law, from one phase of the flight to the next, are are necessary. From a strict optimal control point of view, it is necessary to change all the control gains for each phase of flight and aircraft condition. To avoid many changes, the following approach was adopted:

1) obtain an optimal control law for a nominal condition as a starting point,
2) using realistic non-linear simulations, modify and update this law to account for the various non-linearities in the actuator servomechanisms, hydraulic systems, engine dynamics and the aerodynamic response, as well as to enhance desirable characteristics which may not adequately be reflected in a quadratic cost function,
3) identify a small number of modifications which can be made at each phase of flight to achieve the differing objectives of each mode.

The employment of modern digital design techniques is well-suited to the discrete nature of the MLS position information and the use of digital flight computers. From the point of view of using lower sampling rates, it is also preferable to the approach of designing an analog system whose response is then approximated by a digital system. Thus,

the control law was developed by imbedding the problem of following a specified flight path into the quadratic regulator with disturbances.

Section II describes the state space formulation of the aircraft dynamics and wind models used in the development. Section III formulates the problem as a sampled data regulator with disturbances. Section IV describes the various modes of the system corresponding to the various phases of the final approach and flare. Section V describes the sensors used in the filter formulations. Section VI describes the results obtained from non-linear simulations of the aircraft and the automatic control system under various wind conditions.

II. AIRCRAFT DYNAMICS AND WIND MODELS

The plant model used to develop DIALS was obtained from the perturbation equations of the aircraft dynamics about the desired or selected glideslope and the localizer at the desired airspeed. The wind model and several other state variables were then coupled with the perturbation equations to obtain the complete model. The latter model was used to generate the control law by applying optimal sampled-data control techniques.

During most of the phases of flight considered, the aircraft maintains a level wings attitude with small deviations of bank angle. Thus, the flight condition corresponding to the tracking of the desired glideslope and the localizer was selected as the reference condition about which the perturbation equations were obtained. In this condition, the longitudinal and lateral perturbation equations are decoupled; i.e., small changes in the lateral variables affect the longitudinal variables only as second order effects; conversely, the effect of the longitudinal variables on the lateral motion is also of second order. Thus, the control and modeling of the longitudinal and lateral dynamics were considered separately.

The notation for the coordinate axes used in this study can be established by considering three sets of coordinate axes: the earth fixed axes, the body axes, and the stability axes. The earth-fixed coordinate frame (x_e, y_e, z_e) has its origin fixed at the glidepath intercept point (GPIP) on the runway. The x_e axis is along the runway centerline, the direction in which the aircraft lands being chosen positive

along x_e. The z_e axis is the local vertical, positive downwards; y_e is perpendicular to both x_e and z_e, with its positive end directed so as to make the coordinate frame right-handed. The earth is assumed to be stationary with respect to inertial space; so that the earth-fixed axes form an inertial frame.

The body axes (x_b, y_b, z_b) and the stability axes (x_s, y_s, z_s) are fixed to the body of the aircraft; i.e., they are body-fixed axes. The origin of both axes is fixed at the aircraft center of mass. The x_b axis is along the fuselage reference line of the aircraft, positive towards the nose, the y_b axis is positive towards the tip of the right wing, the z_b axis is perpendicular to both x_b and y_b and is positive downwards (when the aircraft pitch angle is zero). The stability axes (x_s, y_s, z_s) are obtained from the body axes by a rotation of α_o, the steady state angle of attack, about the y_b axis. The three sets of coordinate frames are shown in Figure 2.

A. LONGITUDINAL EQUATIONS

The general equations of motion for rigid aircraft can be linearized about a steady flight condition as described in [7], [8]. The nominal flight condition used here corresponds to flight among the selected glide-slope and localizer, at a constant airspeed with the flaps at 40 degrees and the gear down in the landing configuration. The longitudinal perturbation equations for describing the aircraft's motion in the vertical plane can be expressed in the stability axes as:

$$m\dot{u} = - mg \cos\gamma_o \theta + f_{a_x} + f_{T_x} \qquad (1)$$

$$m(\dot{w} - U_o q) = - mg \sin\gamma_o \theta + f_{A_z} + f_{T_z} \quad (2)$$

$$I_{yy} \dot{q} = m_A + m_T \quad (3)$$

where

U_o - steady inertial speed in the x_s direction

γ_o - glideslope angle

θ - perturbation in pitch angle

q - pitch rate

f_{A_x} - perturbation in net aerodynamic force along the x_s direction

f_{A_z} - perturbation in net aerodynamic force along the z_s direction

f_{T_x} - perturbation in thrust along the x_s direction

f_{T_z} - perturbation in thrust along the z_s direction

m_A - perturbation in pitching moment due to aerodynamic forces

m_T - perturbation in pitching moment due to thrust

I_{yy} - moment of inertia about the y_s axis

m - aircraft mass

u - perturbation in inertial speed along the x_s direction

w - inertial speed along the z_s direction

In equation (1), the term f_{A_x} represents the total algebraic change in the value of the aerodynamic force along the x_s axis due to changes from steady state values in the values of the aerodynamic and control variables; the terms f_{A_z}, f_{T_z}, f_{A_x}, m_A and m_T are defined similarily as the changes in the appropriate forces or moments from their steady values

on the glideslope. These terms can be expressed in terms of the aircraft stability derivatives, the moments of inertia and the perturbations in the aerodynamic and control variables. Substituting these expressions for the force and moments into equations (1) - (3), the aircraft equations of motion can be expressed as given below.

$$m\dot{u} = - mg \cos\gamma_o \theta + \bar{q}_o S\left\{(-C_{D_{\underline{u}'}} + 2C_{D_o} + C_{T_{x\underline{u}'}} + 2C_{T_{xo}}) \underline{u}'\right.$$

$$\left. + (C_{Lo} - C_{D\underline{\alpha}}) \underline{\alpha} - C_{D\delta e} \delta e - C_{D\delta s} \delta s + C_{T_x\delta T} \delta T \right\} \quad (4)$$

$$m(\dot{w} - U_o q) = - mg \sin\gamma_o \theta + \bar{q}_o S \left\{ -(C_{L\underline{u}'} + 2C_{Lo}) \underline{u}'\right.$$

$$\left. - (C_{L\alpha} + C_{Do}) \underline{\alpha} - C_{L\underline{\dot{\alpha}}} \underline{\dot{\alpha}} - C_{L\underline{q}} \underline{q} \right\} \quad (5)$$

$$I_{yy} \dot{q} = \bar{q}_o Sc\left\{ (C_{M\underline{u}'} + 2C_{Mo}) \underline{u}' + (C_{M\underline{\alpha}} + C_{MT\_}) \underline{\alpha} + C_{M\underline{\dot{\alpha}}} \underline{\dot{\alpha}}\right.$$

$$\left. + C_{M\underline{q}} \underline{q} + C_{M\delta e} \delta e + C_{M\delta s} \delta s + C_{M\delta T} \delta T \right\} . \quad (6)$$

where

$$\underline{u}' = \frac{u + u_w}{U_o} \quad (7)$$

$$\underline{\alpha} = \alpha + \alpha_w \quad , \quad (8)$$

$$\underline{q} = q + q_w \quad , \quad (9)$$

u_w, α_w, and q_w are the components due to wind, $\bar{q}_o$ is the steady value of the dynamic pressure at the selected airspeed, S is the effective wing area, δe, δs, and δT are the perturbations of elevator, stabilizer and thrust, respectively.

Equations (4) - (6) describe the linear and angular velocities of the aircraft in the vertical plane. The position of the aircraft can be obtained by integrating the inertial velocity components over time. Thus,

$$\dot{x}_e' = \frac{\dot{x}_e}{U_o} = L_{ES}(1,1)(1 + u') + L_{ES}(1,2)\beta + L_{ES}(1,3)\alpha \quad , \tag{10}$$

$$\dot{z}_e' = \frac{\dot{z}_e}{U_o} = L_{ES}(3,1)(1 + u') + L_{ES}(3,2)\beta + L_{ES}(3,3)\alpha \quad , \tag{11}$$

where $L_{ES}(i,j)$ is the element in i^{th} row and j^{th} column of the matrix, L_{ES}, which represents the transformation from the stability axes to the earth-fixed axes. Note that α and β are inertial quantities and correspond to normalized velocity components in the stability axes; under no wind conditions these would be the same as the aerodynamic angle of attack and sideslip. The position equations can be rewritten in the following form.

$$\dot{x}_e' = -\sin\gamma_o\,\theta + \cos\gamma_o\,u' + \sin\gamma_o\,\alpha + \eta_x \quad , \tag{12}$$

$$\dot{z}_e' = -\cos\gamma_o\,\theta - \sin\gamma_o\,u' + \cos\gamma_o\,\alpha + \eta_z \quad , \tag{13}$$

where

$$\eta_x = L_{ES}(1,1)(1 + u') - \cos\gamma_o\,u' + \sin\gamma_o\,\theta + L_{ES}(1,2)\beta + (L_{ES}(1,3) - \sin\gamma_o)\alpha \quad , \tag{14}$$

$$\eta_z = L_{ES}(3,1)(1 + u') + \sin\gamma_o\,u' + \cos\gamma_o\,\theta + L_{ES}(3,2)\beta + (L_{ES}(3,3) - \cos\gamma_o)\alpha \quad , \tag{15}$$

In this form, the differential equations are linear with a forcing function that contains the non-linear part, which are second order terms with respect to the steady flight conditions considered. With this approach we can use linear theory in the development of the filter and control law without neglecting the non-linear terms completely. To obtain the second order terms for the remaining variables, consider the equations

$$\dot{\theta} = \cos\phi\ q - \sin\phi\ r \quad , \tag{16}$$

$$a_{x_s} = \dot{u} + qw - rv \quad , \tag{17}$$

$$a_{z_s} = \dot{w} - q(U_o + u) + pv \tag{18}$$

Rearranging these equations, we obtain

$$\dot{\theta} = q + \eta_\theta \ , \tag{19}$$

$$\dot{u}' = \frac{a_{x_s}}{U_o} + \eta_{u'} \quad , \tag{20}$$

$$\dot{\alpha} = \frac{\dot{w}}{U_o} = \frac{a_{z_s}}{U_o} + q + \eta_\alpha \ , \tag{21}$$

where

$$\eta_\theta = (\cos\phi - 1)\ q - \sin\phi\ r \quad , \tag{22}$$

$$\eta_{u'} = -\ q\ \alpha + r\ \beta \quad , \tag{23}$$

$$\eta_\alpha = q\ u' - p\ \beta \tag{24}$$

It may be noted that the perturbation equations (4) - (6) neglect the second order terms represented by η_θ, $\eta_{u'}$, and η_α. The second order

terms introduce some coupling between the longitudinal and lateral equations. To model the actuator dynamics and obtain a control rate structure

$$\dot{\delta T} = -.5\ \delta T + .298\ \delta th \quad , \tag{25}$$

$$\dot{\delta th} = u_2 \quad , \tag{26}$$

$$\dot{\delta s} = u_3 \quad , \tag{27}$$

where δT is the thrust perturbation in units of one thousand pounds per unit of δT, δth is the throttle perturbation in degrees and δs is the stabilizer perturbation in radians. As the lags in the elevator action are small, the elevator time constant was neglected. The aircraft's longitudinal equations of motion, the position equations and the actuator equations can be combined and after some manipulation can be expressed in state variable form.

$$x_\ell^T = (\theta \quad u' \quad \alpha \quad q \quad x' \quad z' \quad \delta T \quad \delta th \quad \delta s) \quad , \tag{28}$$

$$u_\ell^T = (\delta e \quad \dot{\delta s} \quad \dot{\delta th}) \quad , \tag{29}$$

$$w_\ell^T = (u_w' \quad \alpha_w \quad q_w) \quad , \tag{30}$$

$$\eta_\ell^T = (\eta_\theta \quad \eta_{u'} \quad \eta_\alpha \quad 0 \quad \eta_x \quad \eta_z \quad 0 \quad 0 \quad 0) \quad , \tag{31}$$

$$\dot{x}_\ell = A_\ell x_\ell + B_\ell u_\ell + D_\ell w_\ell + \eta_\ell \quad , \tag{32}$$

where A_ℓ, B_ℓ, and D_ℓ are matrices of appropriate size corresponding to the coefficients in the original equations. Expressions for the elements of these matrices can be obtained in terms of the stability derivatives of the aircraft.

To complete the model of the longitudinal equations of motion, it is necessary to model the wind velocities which affect the motion of the aircraft as seen in (32).

The longitudinal wind model contains the components of steady wind velocities, turbulence and shear winds in the longitudinal axes. The turbulence model uses the Dryden spectra [4] for the various components varying with altitude. The turbulence model has three components: u_g' in the x_b direction, α_g in the z_b direction, and q_g which models the effect of turbulence on the pitch rate of the aircraft. These components are modeled using the following spectra,

$$S_u(\Omega) = \frac{2\sigma_u^2 L_u}{1 + (L_u\Omega)^2} \quad , \tag{33}$$

$$S_\alpha(\Omega) = \frac{\sigma_w^2 L_w}{V_a^2} \quad \frac{1 + 3(L_w\Omega)^2}{1 + (L_w\Omega)^2\,2} \quad , \tag{34}$$

$$S_q(\Omega) = \frac{\Omega^2 V_a^2}{1 + (\frac{4b}{\pi}\Omega)^2} \quad S_\alpha(\Omega) \quad , \tag{35}$$

where b is the wing span, L_u and L_w are the scales of turbulence, V_a is the airspeed, and Ω is the spatial frequency related to the temporal frequency $\bar{\omega}$ by

$$\Omega = \bar{\omega}/V_a. \tag{36}$$

The u_g' component is independent of α_g and q_g; however, α_g and q_g are correlated with their cross spectral density being

$$S_{q\alpha}(\omega) = \frac{j\omega}{1 + j\,\frac{4b}{\pi V_a}\,\omega}\, S_{\alpha}(\omega) \tag{37}$$

The above spectra can be factored using spectral factorization methods to obtain a linear system driven by white noise which generates an output having the above spectral characteristics [7], [3], [13]. Thus, the following transfer functions are obtained to generate u'_g, α_g and q_g,

$$G_u(s) = \frac{1}{1 + \frac{L_u}{V_a}\,s} \quad , \tag{38}$$

$$G_{\alpha}(s) = \frac{1 + 3\,\frac{L_w}{V_a}\,s}{1 + 2\,\frac{L_w}{V_a}\,s + (\frac{L_w}{V_a})^2\,s^2} \quad , \tag{39}$$

$$G_q(s) = \frac{s}{1 + \frac{4b}{\pi V_a}\,s} \tag{40}$$

where α_g is the input to the system $G_q(s)$ to obtain q_g with the specified spectrum and cross-spectral density. Figure 3 shows block diagrams of the systems generating the turbulence components.

The steady and shear wind in the longitudinal direction was modeled by

$$\dot{u}'_s = u'_{sh} \quad , \quad \dot{u}'_{sh} = \xi_{\ell 3} \quad , \tag{41}$$

$$\alpha_s = \xi_4 \quad . \tag{42}$$

Thus, to simulate a specified shear profile for $\dot{u}'_s$, with appropriate initial conditions, e.g., to obtain a linear profile u'_s changing at a rate of u'_{sho}, the initial conditions for u'_{sh} is set to u'_{sho} and $\xi_{\ell 3}$ is set equal

to zero; alternately, an impulse in $\xi_{\ell 3}$ will also achieve the same profile.

The transfer functions obtained for the wind model can equivalently be expressed as differential equations in state variable form as shown in (43),

$$\dot{W}_\ell = A_{w\ell}\, W_\ell + B_{w\ell}\, \xi_\ell \quad , \qquad w_\ell = C_{w\ell}\, W_\ell \quad , \tag{43}$$

where w_ℓ is given by equation (30). Thus, the coupled equations (32) and (43) model the longitudinal motion of the aircraft under various wind conditions.

B. LATERAL EQUATIONS

The lateral equations of motion were obtained using the same approach as the longitudinal equations. The flight condition about which the general equations of motion were linearized corresponds to flight along the localizer, at the selected glideslope and airspeed, with the flaps at 40 degrees and the gear down in the landing configuration. For this condition, the perturbation equations can be written as

$$m(\dot{v} + U_o r) = mg \cos\gamma_o\, \phi + f_{A_y} + F_{T_y} \quad , \tag{44}$$

$$I_{xx}\, \dot{p} - I_{xz}\, \dot{r} = \ell_A + \ell_T \quad , \tag{45}$$

$$I_{zz}\, \dot{r} - I_{xz}\, \dot{p} = b_A + n_T \quad . \tag{46}$$

Equations (44) - (46) are the perturbation equations which describe the lateral dynamics of the aircraft, where

U_o - steady-state inertial speed along the stability x-axis, i.e., along x_s,

v - perturbation in the inertial speed along the stability y-axis, i.e., along y_s,

p - perturbation in the roll rate about x_s,

r - perturbation in the yaw rate about z_s,

γ_o - steady-state flight path angle,

ϕ - perturbation in the roll angle,

f_{A_y} - perturbation in the net aerodynamic force along y_s,

f_{T_y} - perturbation in the thrust force along y_s,

ℓ_A - perturbation in the rolling moment due to aerodynamic forces,

n_A - perturbation in the yawing moment due to aerodynamic forces,

ℓ_T - perturbation in the rolling moment due to thrust,

n_T - perturbation in the yawing moment due to thrust,

and I_{xx}, I_{zz} and I_{xz} are the moments of inertia of the aircraft in the stability axes.

The terms f_{A_y}, f_{T_y}, ℓ_A, ℓ_T, n_A and n_T can be expressed in terms of the stability derivatives of the aircraft evaluated at the steady state values of the aerodynamic variables and the control surface settings, in linear form [7], [8], [9]. Substituting these expressions into equations (44) - (46) and rearranging terms, we obtain linear differential equations in the sideslip angle, the roll rate and yaw rate. Writing the derivatives of the roll and yaw angles in terms of roll and yaw rates, we obtain the following set of differential equations.

$$\dot{\phi} = \sec\theta_o \, (\cos\gamma_o p + \sin\gamma_o r) \tag{47}$$

$$\dot{\psi} = \sec\theta_o \, (\sin\alpha_o p + \cos\alpha_o r) \tag{48}$$

$$\dot{\beta} = a_{31} \phi + a_{33} \beta + a_{34} p + a_{35} r + b_{31} \delta A + b_{32} \delta R + b_{33} \delta sp + h_{31} \beta_w + h_{32} p_w + h_{33} r_w \tag{49}$$

$$\dot{p} = a_{43}\,\beta + a_{44}\,p + a_{45}\,r + b_{41}\,\delta A + b_{42}\,\delta R + b_{43}\,\delta sp + h_{41}\,\beta_w + h_{42}\,p_w + h_{43}\,r_w \tag{50}$$

$$\dot{r} = a_{53}\,\beta + a_{54}\,p + a_{55}\,r + b_{51}\,\delta A + b_{52}\,\delta R + b_{53}\,\delta sp + h_{51}\,\beta_w + h_{52}\,p_w + h_{53}\,r_w \tag{51}$$

where β, p and r are the sideslip angle, roll rate and yaw rate, respectively, β_w, p_w and r_w are the sideslip angle, the roll rate and yaw rate due to wind velocities only, δA, δR and δsp are the perturbations of the ailerons, rudder and spoilers, respectively. The coefficients a_{ij} in the above equations depend on the aircraft stability derivatives and are given in the Appendix. Thus, a set of linear differential equations describing the lateral velocities and attitude of the aircraft can be obtained.

The position of the aircraft relative to runway centerline is expressed by the perpendicular distance of the aircraft center of mass to the runway centerline. This distance normalized by the aircraft's steady-state speed will be used as a state variable in addition to the equations already obtained. Then, the lateral distance y (in feet) of the aircraft can be expressed by

$$\dot{y} = U_o[L_{ES}(2,1)(1 + u') + L_{ES}(2,2)\beta + L_{ES}(2,3)\alpha] \ , \tag{52}$$

where u' is the normalized inertial perturbation in the speed along the x_s direction and α is the perturbation in the inertial angle of attack, and

$$L_{ES}(2,1) = \cos\alpha_o \cos(\theta_o + \theta) \sin\psi + \cos\phi \sin\alpha_o \sin(\theta_o + \theta) \sin\psi - \sin\alpha_o \sin\phi \cos\psi \tag{53}$$

$$L_{ES}(2,2) = \sin\phi \sin(\theta_o + \theta) \sin\psi + \cos\phi \cos\psi \tag{54}$$

$$L_{ES}(2,3) = -\sin\alpha_o \cos(\theta_o + \theta) \sin\psi + \cos\alpha_o \cos\phi \sin(\theta_o + \theta) \sin\psi$$
$$- \cos\alpha_o \sin\phi \cos\psi \quad . \tag{55}$$

Rearranging the terms in equation (52)

$$\dot{y}' = \beta + \cos(\alpha_o - \theta_o)\psi - \sin\alpha_o \phi + \eta_y \quad , \tag{56}$$

where η_y and y' are given by

$$\eta_y = (L_{ES}(2,2) - 1)\beta + L_{ES}(2,1)(1 + u') - \cos(\alpha_o - \theta_o)\psi$$
$$+ L_{ES}(2,3)\alpha + \sin\alpha_o \phi \quad , \tag{57}$$

$$y' = y/U_o \quad . \tag{58}$$

Note that equation (56) contains no approximation when α in (57) is interpreted as the normalized inertial velocity component in the z_s direction, but is simply a rearranged form of (52) with the non-linear terms grouped into a single term. To obtain the second order terms for the remaining variables, note that

$$\dot{\phi} = \sec\theta_o (\cos\gamma_o p + \sin\gamma_o r) + \eta_\phi \quad , \tag{59}$$

$$\dot{\psi} = \sec\theta_o (\sin\alpha_o p + \cos\alpha_o r) + \eta_\psi \quad , \tag{60}$$

$$\dot{\beta} = \frac{a_{y_s}}{U_o} - r + \eta_\beta \quad , \tag{61}$$

where

$$\eta_\phi = (\cos\phi \tan(\theta_o + \theta) - \tan\theta_o)(\cos\alpha_o r + \sin\alpha_o p) \quad , \tag{62}$$

$$\eta_\phi = (\cos\phi \sec(\theta_o + \theta) - \sec\theta_o)(\cos\alpha_o\, r + \sin\alpha_o\, p) \quad , \tag{63}$$

$$\eta_\beta = p\alpha - ru \quad , \tag{64}$$

when q is assumed to be small.

The servo systems, hydraulic and mechanical actuator systems on this aircraft have clearly noticeable non-linear effects. These effects include usual non-linearities such as hysteresis, rate and position limits, as well as d.c. gain variations as a function of actuator position, dynamic pressure, etc., and non-linear spoiler feedforward and feedback systems. These non-linear effects were not included in the "control design model" described here. However, these non-linearities were included in the simulation model, and design changes were made to accommodate these non-linear effects during the control development using the non-linear simulation and later during the flight tests.

The controls which affect the lateral motion of the aircraft are the aileron, rudder and spoiler surface settings as can be seen from equations (47) - (51), where the spoiler action is used mainly to aid the effect of the ailerons during turns. Thus, the spoiler setting is programmed according to the aileron setting. This is approximated and modeled here as

$$\delta s_p = C_{spa}\ \delta A \quad , \qquad C_{spa} = 1.73 \quad . \tag{65}$$

A rate command structure was used for the rudder control; hence, the rudder position is considered a state variable which is obtained by integrating the rudder rate command.

$$\dot{\delta R} = u_2 \quad , \tag{66}$$

where u_2 is considered to be the rudder rate control.

If the relation between the spoiler and aileron given in (65) is substituted in (49), (50) and (51), then the spoiler terms are eliminated from the equations. Now, forming a state vector x such that

$$x^T = (\phi \quad \psi \quad \beta \quad p \quad r \quad y' \quad \delta R) \tag{67}$$

and a control vector u such that

$$u^T = (\delta A \quad \delta \dot{R}) \quad , \tag{68}$$

equations (47) - (51), (56), (65) and (66) can be combined into a state variable model of the lateral motion of the aircraft of the form

$$\dot{x} = Ax + Bu + Dw + \bar{\eta} \quad , \tag{69}$$

where $w^T = (\beta_w \quad p_w \quad r_w)$ and $\bar{\eta}^T = (\eta_\phi \quad \eta_\psi \quad \eta_\beta \quad 0 \quad 0 \quad \eta_y \quad 0)$.

The lateral motion of the aircraft is described by the state variable model given in equation (69); this model describes the response of the aircraft when a control is applied or when the wind velocities such as gusts or steady winds are non-zero. The effects of the wind velocities are introduced through the vector w. The components of this vector are β_w or the wind velocity along the y_s direction normalized by the airspeed of the aircraft, p_w or the rotation of the air around the aircraft about the x_s axis, and r_w or the rotation of the air around the aircraft about the z_s axis, respectively. The roll rate p_w and yaw rate r_w components of the wind vector w consist only of the effects of wind gusts, thus having an average value of zero; i.e., these components do not have a steady state effect but introduce turbulence effects into the equations. On the other hand, the β_w or the normalized lateral wind velocity contains terms for

both wind gusts and steady winds; thus, it is modeled as

$$\beta_w = \beta_g + \beta_s \quad , \tag{70}$$

where β_g is the gust or turbulence term, and β_s is the steady wind term. The gust terms are of a random nature and can be modeled using the well-known Dryden spectrum [7], [8]. This method consists of using spectral factorization methods to obtain a dynamical system which generates a random process having the specified power spectral density when driven by a white noise process [10], [11], [12], and [13].

The Dryden spectra describe the statistical behaviour of wind gust velocities along the aircraft body coordinates by specifying their power spectral densities in terms of the spatial frequency Ω [14]. The spectra for the gust components of interest are given below.

$$S_\beta(\Omega) = \sigma_v^2 \frac{L_v}{\pi V_a^2} \frac{1 + 3\,(L_v\,\Omega)^2}{[1 + (L_v\,\Omega)^2]^2} \tag{71}$$

$$S_p(\Omega) = \frac{\sigma_w^2}{L_w} \frac{8\,(\frac{\pi L_w}{4b})^{1/3}}{1 + (\frac{4b\,\Omega}{\pi})^2} \tag{72}$$

$$S_r(\Omega) = \frac{\Omega^2\,V^2}{1 + (\frac{3b\,\Omega}{\pi})^2} \quad S_\beta(\Omega) \quad , \tag{73}$$

where b is the wing span, L_v and L_w are the scales of turbulence, V_a is the airspeed, σ_v^2 is the variance of the lateral gust and σ_w^2 is the variance of the vertical gust. The change from the spatial frequency Ω to the temporal frequency $\bar{\omega}$ can be made by

$$\Omega \equiv \frac{\bar{\omega}}{V_a} \tag{74}$$

Substituting equation (74) into the expressions for the power spectral densities of the wind gusts, we obtain the spectra in terms of the temporal frequency; then using spectral factorization techniques the following transfer functions can be obtained

$$G_\beta(s) = -\sigma_v \left[\frac{L_v}{\pi V_a^3}\right]^{\frac{1}{2}} \frac{1 + \frac{3 L_v s}{V_a}}{(1 + \frac{L_v s}{V_a})^2} \quad , \tag{75}$$

$$G_p(s) = \sigma_w \left[\frac{1}{L_w V_a}\right]^{\frac{1}{2}} \frac{\left[8(\frac{\pi L_w}{4b})\frac{1}{3}\right]^{\frac{1}{2}}}{1 + \frac{4b s}{\pi V_a}} \quad , \tag{76}$$

$$G_r(s) = \frac{-s}{1 + \frac{3b s}{\pi V_a}} \; G_\beta(s) \quad . \tag{77}$$

It should be noted that even though p_w is independent of β_w and r_w, the latter two are not independent of each other. Thus, if a white noise process is input to the transfer function $G_r(s)$, the output would have the desired power spectral density, but may not have the desired cross-correlation with β_g. Hence, equation (77) must be interpreted as β_g being the input to the first term in the above equation in order that the proper cross-correlation be obtained.

The wind gust terms can thus be simulated by passing white noise through the systems with the transfer functions given in equations (75), (76) and (77). The lateral wind, however, has a steady or average value which is not necessarily negligible. Thus, consider that a steady wind is present; in the earth-fixed coordinate system, the wind velocity has a component in the direction of runway centerline W_x, and a component

perpendicular to the runway centerline say W_5; it is assumed that there is no steady wind in the vertical direction although gusts may be present. Hence, if L_{SE} is the transformation matrix from earth-fixed to stability coordinates, then the steady component, β_s, of the normalized lateral wind velocity is given by

$$\beta_s = L_{SE}(2,2)\ W_5 + L_{SE}(2,1)\ W_x \quad , \tag{78}$$

$$L_{SE}(2,1) = \sin(\theta_o + \theta)\ \sin\phi\ \cos\psi - \cos\phi\ \sin\psi \quad , \tag{79}$$

$$L_{SE}(2,2) = \sin(\theta_o + \theta)\ \sin\phi\ \sin\psi + \cos\phi\ \cos\psi \quad . \tag{80}$$

To include wind shear into the model, the steady lateral wind velocity can be described as

$$\dot{W}_5 = W_6 + \omega_3 \quad , \tag{81}$$

$$\dot{W}_6 = \omega_4 \quad , \tag{82}$$

where ω_3 and ω_4 are gaussian white noise processes independent of each other and of β_g, p_w and r_w. Now, the transfer function for the gusts described in (75), (76) and (77) can be combined into a state variable model of fourth order. Adding (81) and (82) to this model, we obtain a sixth order model of the form

$$\dot{W} = A_w\ W + B_w\ \omega \quad , \tag{83}$$

where β_w can be expressed as

$$\beta_w = \beta_g + \beta_s = W_1 + W_5 + \xi_1 \tag{84}$$

$$\xi_1 = (L_{SE}(2,2) - 1)W_5 + L_{SE}(2,1)W_x \quad . \tag{85}$$

Defining the remaining elements of the vector ξ to be zero, w can be written as

$$w = C_w W + \xi \tag{86}$$

This expression can now be subsituted into (69) to obtain

$$\dot{x} = Ax + Bu + DC_w W + \eta \tag{87}$$

$$\eta = D\xi + \bar{\eta} \tag{88}$$

The model for the lateral dynamics, including the aircraft aerodynamics, the actuators and wind conditions, is given by (87) and (83).

III. PROBLEM FORMULATION

The mathematical models obtained in the last section can be used to formulate a discrete stochastic optimal control problem for the design of a digital automatic landing system. The solution to this optimal control problem was used as an initial design in the development of DIALS. Although some modifications to the design were made to account for non-linearities and other unmodeled effects, the basic structure of the optimal control law was left unchanged.

The design problem was formulated as a discrete stochastic quadratic regulator with random disturbances [4], [5], [6]. The longitudinal and lateral control laws were obtained separately, but using the same basic approach. As seen from (32), (43), and (87), (83), the state variable form of both the longitudinal and lateral models is the same; so that either model can be expressed as

$$\dot{x} = Ax + Bu + DC_w W + \eta \quad , \tag{89}$$

$$\dot{W} = A_w W + B_w \omega \quad . \tag{90}$$

To obtain a constant gain control law for the various phases of the final approach and landing, the desired trajectory was modeled in the form

$$\dot{z} = A_z z + \zeta_z \quad , \tag{91}$$

$$\dot{\zeta}_z = \xi_z \quad , \tag{92}$$

where ξ_z is assumed to be a white noise process. The desired trajectory, $z(t)$, is thus modeled as a random process whose statistical properties are

determined by (91), (92). The assumption of a random trajectory is a conceptually appealing one, as it stresses the fact that the trajectory may be altered at any time; the future values of the trajectory are thus not certain, but can be predicted using the model of the trajectory. In general, for an arbitrary deterministic trajectory, the optimal control depends on future values of the trajectory [15], except when the trajectory can be expressed as the output of a homogeneous dynamic system.

The error in the actual trajectory, x(t), can now be defined as

$$e(t) = x(t) - z(t) \quad . \tag{93}$$

The models of the aircraft dynamics (89), (90) and the desired trajectory (91), (92) can be combined, and expressed in terms of the trajectory error, e(t), in the form

$$\dot{e} = Ae + Bu + DC_w W + (A - A_z)z - \zeta_z + \eta \quad , \tag{94}$$

$$\dot{W} = A_w W + B_w \omega \quad , \tag{95}$$

$$\dot{z} = A_z z + \zeta_z \quad , \tag{96}$$

$$\dot{\zeta}_z = \xi_z \quad , \tag{97}$$

$$\dot{\eta} = \xi_\eta \quad , \tag{98}$$

where ω, ξ_z and ξ_η are assumed to be gaussian white noise processes.

Rearranging the terms in (94) - (98),

$$\dot{e} = Ae + Bu + \bar{D}d \quad , \tag{99}$$

$$\dot{d} = A_d d + \xi \quad , \tag{100}$$

where

$$d^T = (W^T \; z^T \; \zeta_z^T \; \eta^T)^T \quad , \tag{101}$$

and ξ is a white noise vector. In (99), (100), the disturbance form of the problem is apparent, where the disturbance, d, is uncontrollable by u, and is the output of a marginally stable system.

A cost function quadratic in the error, e(t), of the form

$$J_c = \frac{1}{2t_f} \int_o^{t_f} E\left\{ e^T(t) \; Q \; e(t) + u^T(t) \; R \; u(t) \right\} dt \tag{102}$$

was selected for the initial design. To obtain a discrete control law for digital implementation, the usual assumption of a constant control between sampling instants was made.

$$u(t) = u_k \quad , \quad kT_o \leq t < (k+1)T_o \quad . \tag{103}$$

With the assumption of (103), the system equations in (99) and (100), and the cost function in (102) can be expressed in terms of the state variables at the sampling instants [16].

$$e_{k+1} = \phi e_k + \Gamma u_k + \Gamma_d \; d_k + \xi_{1k} \quad , \tag{104}$$

$$d_{k+1} = \phi_d \; d_k + \xi_{2k} \tag{105}$$

where e_k and d_k represent the samples $e(kT_o)$ and $d(kT_o)$, and ξ_{1k}, ξ_{2k} are white noise sequences. Similarly, the cost function (102) can be discretized in the form

$$J = \frac{1}{2(N+1)} \; E\left\{ \sum_{k=0}^{N} \left[e_k^T \hat{Q} \, e_k + u_k^T \hat{R} \, u_k + 2 \, e_k^T \hat{N} \, d_k + 2 \, e_k^T \hat{M} \, u_k \right.\right.$$

$$\left.\left. + 2 \, d_k^T \hat{S} \, u_k \right] \right\} . \qquad (106)$$

It is important to note that the discrete cost J and the continuous cost J_c differ by a constant independent of the control sequence used. Thus, to find the control sequence which minimizes the continuous cost J_c, it suffices to obtain the control which minimizes J. The control which minimizes the cost J subject to the constraints of (104) and (105), is given by [6],

$$u_k = -H_{1k} \, \bar{e}_k - H_{2k} \, \bar{d}_k \quad , \qquad (107)$$

where $\bar{e}_k$ and $\bar{d}_k$ are the least mean-square estimates of e_k and d_k, respectively, given past and current measurements, and the gains H_{1k} and H_{2k} are given by

$$H_{1k} = \hat{R}_k^{-1} \, G_{1k} \quad , \quad H_{2k} = \hat{R}_k^{-1} \, G_{2k} \quad , \qquad (108)$$

$$G_{1k} = \Gamma^T \, P_{1k} \, \phi + \hat{M} \quad , \quad G_{2k} = \Gamma^T \, D_k + \hat{S} \quad , \qquad (109)$$

$$D_k = P_{1k} \, \Gamma_d + P_{2k} \, \phi_d \quad , \quad \hat{R}_k = \hat{R} + \Gamma^T \, P_{1k} \, \Gamma \quad , \qquad (110)$$

while P_{1k} and P_{2k} are given by the nonlinear difference equations:

$$P_{1k-1} = \phi^T \, P_{1k} \, \phi - G_{1k}^T \, \hat{R}_k^{-1} \, G_{1k} + \hat{Q} \quad , \quad P_{1N} = \hat{Q} \quad , \qquad (111)$$

$$P_{2k-1} = [\phi - \Gamma \, \hat{R}_k^{-1} \, G_{1k} \,]^T \, D_k + \hat{N} \, , \quad P_{2N} = \hat{N} \quad , \qquad (112)$$

Thus, over a finite optimization interval t_f or N, the optimal control law is specified by (107) - (112). It should be noted that the gain H_{1k} and the cost matrix P_{1k} are the optimal solutions to the LQG problem without any disturbance; i.e., $d_k = 0$. As the optimization interval N increases,

it is well-known that $H_{1k} \rightarrow H_1$; and $P_{1k} \rightarrow P_1$, under loose conditions [17], where the closed-loop system matrix $\phi - \Gamma H$, is stable. If the disturbance matrix ϕ_d satisfies $\rho(\phi_d) \leq 1$, it can be shown that $P_{2k} \rightarrow P_2$ as the optimization interval N increases without bounds, and the cost, J, converges to a finite value. It should be noted that, due to the random plant noise added at every sample, the averaging of the cost over the optimization interval is ncessary to maintain a finite stochastic cost in any (stochastic) LQG problem. The gains H_1 and H_2 can then be obtained by solving (108) - (112). Using these steady state gains, the control law in (107) can be rewritten as

$$u_k = - H_e \bar{e}_k - H_w \bar{W}_k - H_z Z_k - H_\zeta \zeta_k - H_\eta \bar{\eta}_k \quad , \qquad (107\ a)$$

where the control gains for each term in d_k are shown explicitly.

IV. DEVELOPMENT OF THE CONTROL LAW

The main objective of the development was to investigate a direct-digital-design using modern control techniques that would lead to flight tests of the automatic landing system designed on the TCV B-737 Research Aircraft*. The phases of the final approach and landing considered were the localizer and glideslope capture and track, crab/decrab and flare to touchdown. The range of flight conditions considered was 2.5° - 5.5° for glideslope angle, 115 - 135 knots for airspeed, 70,000 - 90,000 lbs for aircraft weight, .2 - .3 for c.g. location, and crosswinds below 15 knots.

The main considerations in the development of DIALS include the overall smoothness of the flight during the final approach, low overshoots of the localizer and glideslope, quick settling on the trajectory and accurate tracking in adverse weather conditions including gusts and shear winds. However, the relative importance of these desirable characteristics varies with the phase of the final approach considered. For example, low overshoot characteristics under differing wind conditions are particularly important during the localizer and glideslope capture maneuvers whereas the actual capture path is of secondary importance; however, during the flare maneuver, the vertical path error is more significant, and, in particular, the touchdown pitch attitude must be sufficiently positive to avoid landing on the nose gear. Similarly, when tracking the localizer and glideslope, it is important to avoid any offsets and have low sensitivity to wind gusts. A more detailed description of the desirable characteristics in the various

*The DIALS flight tests were completed in December 1981. The flight data and test results will be described in a separate report.

control modes is given in the following. To achieve these varying objectives, it appears that some changes in the control law, from one phase of the flight to the next, are necessary.

Some of the differing objectives for each phase of the final approach can be accommodated by different values of the weighting matrices (Q, R) in the cost function. However, in an optimal control design, this would necessitate changing all of the gains of the control law at the initiation of each mode, along with possible transient problems due to switching gains. To avoid possible complexity, the approach taken was to obtain a basic design considering the total trajectory, and then vary a small number of gains using easy-on's and to modify the structure by switching integrators in or out appropriately, at the initiation of each mode. Thus, the basic design model does not contain any integrators; however, when the objective requires it, integrators are switched in or out. For example, at the initiation of the localizer (or glideslope) track mode, the integral of the lateral (or vertical) offset is introduced to obtain a type 1 system without steady offsets. Thus, the basic design is obtained as a stable closed-loop system to which modifications are switched in or out at each mode according to the main objectives of that mode. The specific modifications made at each phase are detailed below.

Non-linearities in the system and unmodeled effects in the aerodynamic characteristics, actuator systems, sensors and electronics were simulated in as much detail as available to obtain a realistic computer simulation of the overall system. These effects were then reduced or eliminated through simulation analyses.

Thus the approach to the overall design of the digital automatic landing system (before flight tests) was:

1) obtain an optimal control law for a nominal condition as a starting point,

2) using realistic non-linear simulations, modify and update this law to account for the various non-linearities in the actuator servomechanisms, hydraulic systems, engine dynamics, and the aerodynamic response, as well as to enhance desirable characteristics which may not adequately be reflected in a quadratic cost function,

3) identify a small number of modifications which can be made at each phase of flight to achieve the differing objectives of each mode.

It should also be noted that the cost function (102) penalizes the error in the actual trajectory relative to the desired trajectory; however, it also penalizes the total control u. As noted in [6], such a cost function does not necessarily provide sufficient trim unless the cost matrices are appropriately selected or the control cost is modified to penalize the deviation from a pre-selected trim [18]. For example, consider the action of the elevator and stabilizer. On the TCV B-737 Research Aircraft, the effects of the elevator and stabilizer on the motion of the aircraft are the same, except that the effectiveness of the larger stabilizer surface is twice that of the elevator. It is desirable to make trimming changes using the stabilizer, and maintain the elevator near its equilibrium position (referenced at 0) to avoid high moments on the elevator hinge over sustained periods of time. Of course, the fast motion (due to the actuators) of the elevator is used to stabilize the dynamic modes of the aircraft. Since the trim values required on different glideslopes, or wind conditions, or c.g.

locations, etc. vary with the particular condition encountered, it is desirable to have the stabilizer position move to trim the aircraft, while the elevator is maintained at low hinge moment values except in transients. Thus, it is desirable not to penalize stabilizer position, but to penalize elevator position to obtain the desired trimming action. Since, it is also desirable (and necessary) to have slow stabilizer motion, high stabilizer rate should be appropriately penalized to obtain smoother transitions. Thus, appropriate selection of the cost matrices with rate command structure can provide appropriate trimming with optimal control formulation described in the previous section. Similarly, throttle position is not penalized, while a non-zero penalty on throttle rate provides smoother and slower autothrottle action. In general, control activity can be placed at desirable levels by penalizing the control rate.

To obtain a 3-D control law, the variable corresponding to distance along runway centerline ($x_{\ell 5}$) was eliminated from the equations of motion for the design model. However, the filter development model included (and estimated) this variable.

The specific modification used at the initiation of the various modes of the automatic landing system are described in the following sections.

A. LOCALIZER CAPTURE

The main function during the localizer capture mode is to perform a smooth transition from the aircraft's initial position to the runway centerline, so that the aircraft can quickly settle and stabilize on the localizer. Two important characteristics were stressed in the design and development of DIALS for this mode.

The first characteristic is the reduction of overshoots of the localizer and the settling time under adverse weather conditions. Consistently low overshoots of the localizer are particularly important in airports with close parallel runways. This property can be used to increase the efficiency of the terminal area as it allows the two parallel runways to be operated independently. A low overshoot also reduces the settling time on the localizer, thus allowing close-in captures when necessary.

The second characteristic is to initiate the capture maneuver by rolling the aircraft away from the runway centerline. Pilots usually initiate localizer capture in this fashion, and consider rolling towards the runway centerline "the wrong direction". Thus, this characteristic makes pilot monitoring of the capture easier, as it is the expected behaviour. This property can be obtained by initiating the localizer capture when the natural tendency of the control law is to roll in the desired direction. To achieve this property, consider the component of u_k in (107a) corresponding to the aileron command. The distance, y_k, from the localizer at which the aileron command crosses zero was selected to initiate the localizer capture mode. Assuming level wings and using the initial conditions for the filter states, and neglecting small terms, a localizer capture criterion of the following form can be obtained

$$|\bar{y}_k| < U_o|c_1 \bar{\psi}_k + c_2 \bar{\beta}_k + c_3 \bar{\beta}_{wk}| \quad , \tag{113}$$

$$c_1 = H_{e\,1\,2}/H_{e\,1\,6} \quad , \quad c_2 = H_{e\,1\,3}/H_{e\,1\,6} \tag{113 a}$$

$$c_{1\,3} = (H_{w\,1\,5} + H_{\zeta\,1\,3} A_{3\,3} + H_{\zeta\,1\,4} A_{4\,3} + H_{\zeta\,1\,5} A_{5\,3} + H_{\zeta\,1\,6} A_{6\,3})/H_{e\,1\,6} \tag{113 b}$$

where $\bar{y}_k$, $\bar{\psi}_k$, $\bar{\beta}_k$, and $\bar{\beta}_{wk}$ are estimates of the distance from runway centerline, the heading relative to the runway, the inertial normalized side velocity and the normalized cross-wind velocity, respectively.

The localizer capture mode is initiated when the inequality holds. The constants are chosen so that the initial tendency is to roll away from the localizer with the possible exception of conditions when the aircraft is already rolled as desired, say due to gusting winds. It should be noted that the localizer capture mode is engaged farther away from the runway centerline when the desired speed U_o is higher, as would be expected. To further ensure a smooth transition, an "easy-on" function was used on the aileron command signal.

To avoid large overshoots beyond the runway centerline, appropriate closed-loop damping of the control law was obtained by proper selection of the weighting matrices Q and R and simulation of the localizer capture.

B. GLIDESLOPE CAPTURE

The desirable properties of the glideslope capture mode include low overshoot and the tendency to pitch down at the initiation of the capture. To have a low overshoot of the glideslope for the various steep glideslope angles that may be selected (i.e., 2.5° - 5.5°), it is desirable to initiate the capture when the aircraft is well below the glideslope. This approach is different than the practice of engaging the glideslope hold mode when the glideslope is intercepted (e.g., see [9]), where an overshoot, even if small, cannot be avoided.

Initiation of the capture mode below the glideslope alone does not guarantee a low overshoot. Thus, some experimentation in the selection

of the weighting matrices coupled with simulation was used to achieve this property. In particular, for both overshoot characteristics and smoothness of maneuver, the sink rate command was eased on from zero to the glideslope sink rate. This implementation provides a simple method of adjusting the speed with which the capture maneuver is performed without an appreciable overshoot.

While engaging the capture mode below the glideslope is desirable for overshoot characteristics, it also produces an initital tendency for the aircraft to pitch up. To avoid this effect, the capture engage logic was selected so that the initial tendency of the elevator is to produce a negative pitching moment.

To achieve this property, consider the component of u_k, in (107a), corresponding to the elevator command. If the glideslope capture mode is engaged at the altitude, h_{GSC}, where the elevator command crosses zero, it can be seen that the initial elevator command will tend to gradually produce a negative pitching moment.

While the thrust also has a considerable contribution to the pitching moment in this aircraft, due to the engine location, the DIALS autothrottle and engine dynamics have much longer time constants than those associated with the elevator. Thus, changes in the throttle command and thrust are of small magnitude over short period of time, so that the initial pitching tendency is determined by the faster elevator command. Although the initial tendency of the DIALS throttle command is to lower the thrust level, which is the desirable action, the glideslope capture criterion was selected by considering only the elevator action. After some manipulation, and neglecting terms of small magnitude, the following glideslope capture altitude can be obtained.

$$h_{GSC} = -\tan\gamma_o \bar{x}_e - U_o \left[c_{\ell 1} \bar{e}_{\ell 1} + c_{\ell 2} \bar{e}_{\ell 2} + c_{\ell 3} \bar{e}_{\ell 3} + c_{\ell 7} \bar{e}_{\ell 7} + c_{\ell 8} \bar{e}_{\ell 8} + c_{\ell 9} \bar{e}_{\ell 9} + d_{\ell 3} z_{\ell 3} \right] \quad (114)$$

$$c_{\ell i} = \frac{H_{e_\ell\ 1\ i}}{H_{e_\ell\ 1\ 6}} \quad , \qquad i = 1, 2, 3, 7, 8, 9 \quad , \quad (114\ a)$$

$$d_{\ell 3} = \frac{H_{z_\ell\ 1\ 3}}{H_{e_\ell\ 1\ 6}} \quad , \quad (114\ b)$$

where γ_o is the selected glideslope angle, $\bar{x}_e$ is the estimated ground distance to the glide path intercept point (GPIP), $\bar{e}_i$ is the estimated error in the state x_i, and $z_{\ell 3}$ is the commanded inertial angle of attack. Note that, as in the localizer capture, the glideslope capture altitude is lower when the desired speed is higher. Further note that the criterion is applicable to the capture of an arbitrary glideslope by using the glideslope angle selected by the pilot as γ_o in (114).

C. LOCALIZER AND GLIDESLOPE TRACK

As the aircraft gets closer to the localizer or glideslope, the localizer or the glideslope track (or hold) modes are engaged, the order depending on the particular approach path. In comparison to the capture modes, the main objectives considered in the design of the track modes were to achieve quick settling on the localizer and glideslope, insensitivity to wind disturbances (gusts, shear and steady winds), and accurate tracking of the localizer and glideslope.

Since it is not desirable to start the flare maneuver before the aircraft is fully stabilized on the glideslope, a low settling time for the track modes is important to enable "close-in captures". The capability

to accurately capture and track a shallow or steep glideslope provides a flexibility which can be used to avoid vortices when following large aircraft, reduce the noise perceived by airport communities, and generally increase terminal area operations efficiency.

The localizer track mode is engaged when the aircraft is 30 ft. from the runway centerline or 25 seconds after the localizer capture has been engaged. Since the main objective of the track mode is to minimize excursions away from the runway centerline, the gains feeding back the cross-track error estimate to the aileron and rudder are increased gradually for a smooth mode transition. Since a type 1 system is desirable in this mode, an integrator for the cross-track error is also initiated to avoid steady state offsets from the runway centerline. Initially, the integrator gains were set equal to a tenth of the gains for the cross-track error, i.e., the product of the sampling interval and the cross-track error-gain. The gains were then adjusted using simulation results to improve the performance under the various conditions expected to occur.

The glideslope track mode is engaged when the aircraft intercepts the glideslope, or 25 seconds after the glideslope capture mode has been engaged. The latter criterion is used to ensure that the track mode is engaged even if the aircraft does not overshoot and cross the glideslope. To reduce any excursions from the selected glideslope, the gains feeding back the deviation from the glideslope and the error in the normalized vertical velocity are increased gradually using an easy-on. To avoid steady state offsets from the glideslope, an integrator on the glideslope deviation is introduced when the track mode is initiated.

During both the capture and track modes, the DIALS filters estimate

the components of the wind velocities. These estimates are fed to the controller to compute the surface command signals. Thus, to the extent that the wind velocities are estimated, the control law performs a gust alleviation function; i.e., even if no position or inertial velocity errors are present, the wind velocity estimates will produce surface commands which tend to counteract the effects of winds, thus reducing excursions away from the glideslope. The wind velocity estimates are also used to mainatin a constant airspeed. This is obtained by commanding an inertial speed deviation equal to the negative of the wind estimate in the along-track direction. The commanded airspeed thus remains constant at the desired nominal value.

$$z_{\ell 2k} = - \varepsilon_1' \, C_{w\ell} \, W_{\ell k} \quad , \tag{115}$$

$$\zeta_{\ell 2k} = - \varepsilon_1' \, C_{w\ell} \, A_{w\ell} \, \bar{W}_{\ell k} \quad . \tag{116}$$

D. CRAB AND DECRAB

When a cross-wind component is present, it is desirable to control the yaw angle so that the aircraft is headed into the wind with level wings and has no sideslip while remaining on the localizer; i.e., it is desirable to "crab" into the wind. If this condition is not specifically accommodated, an optimal quadratic regulator will usually both yaw and roll into the wind, thus having a non-zero steady state sideslip angle, which is not desirable from the pilot's point of view, while the bank angle can be uncomfortable. To obtain the crab condition in DIALS, a roll integrator is fed back when the aircraft roll reaches 2°, provided that the localizer track mode has been engaged. This ensures a zero

steady state roll angle forcing the yaw angle to automatically adjust itself to the angle necessary for crab. To obtain crab with a quick and smooth transient response, the commanded (aerodynamic) sideslip angle is set to zero, i.e.,

$$z_3 = - \bar{\beta}_{ws} \tag{117}$$

where z_3 is the normalized lateral velocity (inertial sideslip) and $\bar{\beta}_{ws}$ is the estimate of the steady wind velocity. As minimizing the sideslip is desirable in all the phases of flight, except for decrab, the commanded sideslip angle is set to zero at localizer capture initiation and remains active until decrab.

During decrab the aircraft heading is aligned with the runway centerline, while the roll angle is used to maintain the aircraft on the localizer. The decrab mode is initiated at an estimated altitude of 250 ft. It should be noted that this decrab altitude was somewaht arbitrarily selected, and can be reduced to initiate the maneuver at a lower altitude. To obtain the decrab maneuver, first the commands which produce the crab condition are phased out; the roll integrator is phased out and the inertial sideslip command z_3 is set to zero gradually. Since this corresponds to a non-zero commanded aerodynamic sideslip angle, the wind velocity estimates fed into the controller produce a decrab tendency. To enhance this tendency and ensure decrab as a steady state condition, an integrator of the heading relative to the runway is introduced to aid the aileron and rudder actions necessary for decrab. Initially the integrator gains were set equal to a tenth of the heading error gains. These were later adjusted using simulation results to improve the performance throughout the flight regime.

E. FLARE

During the flare maneuver, the main objectives are to reduce the aircraft's sink rate to an appropriately lower level and to touch down with a sufficient margin on the pitch attitude, aligned with the runway, near the selected touch-down point. As DIALS is required to flare from steeper glideslopes than usual for a B-737, the aircraft has a higher sink rate than usual on the glideslope. The approach taken was to generate a flare trajectory on line as a function of the glideslope angle, the desired touch-down flight path angle and the touch-down point; so that when the glideslope is steeper, the flare (initiation) altitude is higher. It should be noted that, for a given approach, the flare path is fixed in space, and is fed to the automatic control system as the desired or commanded trajectory.

The family of flare paths was developed starting from the desired vertical acceleration profile. The following form was selected for this purpose

$$h''(x_e) = \begin{cases} \dfrac{1+\cos 2\Pi(x_e+\Delta X_f)\ /P}{2(H_f - X_f \tan \gamma_o)} & , \quad 2|x_e+\Delta X_f| < P \\ 0 & , \quad \text{otherwise}^* \end{cases} \tag{118}$$

$$P = 2\,\frac{H_f - X_f \tan \gamma_o}{\tan \gamma_{td} - \tan \gamma_o} \quad , \tag{119}$$

$$\Delta X_f = (P - 2\,X_f)/2 \quad , \tag{120}$$

*The prime " ' " denotes differentiation with respect to the distance variable x_e.

where x_e is the x-coordinate of the aircraft's position vector, X_f the touchdown point, H_f the altitude at X_f (zero for touchdown), γ_o and γ_{td} the selected flight path angles on the glideslope and at touchdown, respectively. The desirable characteristics of this profile included the smoothness of transition (e.g., h", hence $\ddot{h}$, has a continuous first derivative at flare initiation), the simplicity of the parametric form (i.e., flare profiles from various glideslopes are obtained according to the value of γ_o), and the case with which h" can be integrated analytically to obtain an expression for h' and h to determine an altitude profile for flare.

It is of interest to note that the flare profile described above was selected after some experimentation with an altitude versus x_e profile of exponential form. These formulations resulted in undersirable transient behaviour at flare initiation, presumably due to the discontinuity in the commanded vertical acceleration when starting flare. The cosine type acceleration profile provides a smooth transition in this variable, while incorporating all the parameters of interest in the flare path such as glideslope angle, touchdown point, etc. For a constant ground speed, $\dot{x}_e$, the vertical acceleration profile is seen to be

$$\dot{h}(x_e) = \dot{x}_e \, h'(x_e) \quad , \tag{121}$$

$$\ddot{h}(x_e) = \dot{x}_e^2 \, h''(x_e) \quad . \tag{122}$$

The vertical profile $h(x_e)$, $\dot{h}(x_e)$, $\ddot{h}(x_e)$ is used in the desired path or command vectors, z_ℓ and ζ_ℓ in order to follow the flare path for the selected glideslope. However, the altitude profile alone does not guarantee all of the desirable and critical properties necessary for an acceptable touchdown. The pitch attitude at touchdown is of utmost importance. A

negative pitch angle at touchdown would result in the nose gear touching down before the landing gear and being subjected to high levels of loading. Thus, a positive pitch angle safety margin is usually desirable. It is also usual to have a decreasing airspeed profile during flare to aid the pitch profile during flare, as well as ease the touchdown speed, sink rate and rollout. To obtain these characteristics the command variables z_ℓ and ζ_ℓ were set as follows.

$$z_{\ell\ 1\ k+1} = z_{\ell\ 1\ k} + .1\ z_{\ell\ 4\ k} \tag{123}$$

$$z_{\ell\ 2\ k+1} = -\ \varepsilon_1^T\ C_{w\ell}\ W_{\ell\ k+1} + DELVF_k \tag{124}$$

$$DELVF_{k+1} = DELVF_k - .1\ DELVFR/U_o\ , \qquad \text{if } DELVF_k \leq -25/U_o \tag{125}$$

$$z_{\ell\ 3\ k+1} = -\ \frac{(\bar{L}_{3\ 1} + \tan\gamma_{d\ k+1}\ \bar{L}_{11})(1+z_{\ell\ 2\ k+1}) + (\bar{L}_{3\ 2} + \tan\gamma_{d\ k+1}\ \bar{L}_{12})\bar{\beta}_{k+1}}{\bar{L}_{1\ 3} + \tan\gamma_{d\ k+1}\ \bar{L}_{1\ 3}} \tag{126}$$

$$z_{\ell\ 4\ k+1} = \frac{U_o\ h''_{k+1}\ \bar{\dot{x}}^2_{e\ k+1}}{\cos(\alpha_o - \bar{\theta}_{k+1})} \tag{127}$$

$$z_{\ell\ 6\ k+1} = Z'_{ed\ k+1} + \tan\gamma_o\ \hat{x}_{\ell\ 5\ k+1} \tag{128}$$

$$\zeta_{\ell\ 1\ k} = 0 \tag{129}$$

$$\zeta_{\ell\ 2\ k} = -\ \varepsilon_1^T\ C_{w\ell}\ A_{w\ell}\ W_{\ell k} - DELVFR \cdot GEZ5/U_o \tag{130}$$

$$\zeta_{\ell\ 3\ k} = 0 \tag{131}$$

$$\zeta_{\ell\ 4\ k} = G_{\zeta_4}\ U_o^2\ \bar{\dot{x}}^3_{ek}\ h'''_k / \cos(\alpha_o - \bar{\theta}_k) \tag{132}$$

$$\zeta_{\ell\ 6\ k} = \dot{z}_{\ell\ 6\ k} + z_{\ell\ 1\ k} - \sec\gamma_o\ z_{\ell\ 3\ k} \tag{133}$$

$$\dot{z}_{\ell\ 6\ k} = (\tan\gamma_o - \tan\gamma_{d\ k})\ \bar{\dot{x}}_{e\ k} \tag{134}$$

where $\gamma_{d\,k}$ is the desired flight path angle at time t_k, GEZ5 is an easy-on, $Z'_{ed\,k}$ is the desired altitude in the earth coordinate axes, $\tilde{L}_{ij}$ is the estimate of $L_{ES}(i,j)$, and ε_1 is the first column of the identity matrix. DELVFR and G_{ζ_4} are constants which can be set according to the amount of decrease in airspeed and the pitch profile desired, respectively. These values were also modified using the profiles obtained in simulation runs.

F. FILTER DEVELOPMENT

As seen in (107), the full state feedback LQG problem requires estimates of all the state variables in its implementation. As the states corresponding to the desired trajectory are known, these variables are not estimated. However, the aircraft motion variables and, in particular, the wind velocity variables including steady winds, shear winds and gusts are required for quick control adjustments to changing wind conditions in the full state feedback formulation*.

The MLS position information and the on-board sensor signals are fed to the longitudinal and lateral DIALS filters shown in Fig. 4 and 5. The filtered estimates are then used to compute the control surface commands as well as to define the desired path. The form of filter used is a discrete Kalman filter with constant gains. The steady state Kalman filter gains were obtained as a starting point, then some gains were modified to obtain better performance using a non-linear simulation of the aircraft. The use of constant gains for the Kalman filters reduces the considerable computation requirements imposed by the error covariance updates. The use

*The author's recent development of a fast, reliable and convergent algorithm for the stochastic output (limited state) feedback problem has made the use of optimal dynamic compensation along with complementary filters practical, and more desirable in high order problems [19].

of discrete filters along with digital controls is well suited to the discrete nature of MLS guidance system. The goals of the filter development include the accurate estimation of the aircraft's position, velocity, attitude and wind velocities using on-board sensors usually available on commercial aircraft, but without using costly inertial platforms, and angle of attack or sideslip sensors which are not currently available on many aircraft.

The aircraft's position is obtained using the MLS guidance system, which provides volumetric coverage in the terminal area. The aircraft receives range, azimuth and elevation information at discrete intervals from which it can obtain its position with high accuracy even under adverse weather conditions. The ground azimuth antenna is located at the runway centerline with coverate up to ±60°. The DME antenna which provides the range of the aircraft is generally co-located with the azimuth antenna. If the DME is located to the side of the runway, a simple transformation can be used to obtain the aircraft's position. The elevation antenna is located at the glidepath intercept point (GPIP), but is offset to the side of the runway; it provides the aircraft's elevation angle up to 20°. Thus, the aircraft has accurate position information in the volume of space within the limits mentioned above.

Consider a right handed coordinate frame with its origin at the phase center of the azimuth anetnna, the x-axis along runway centerline and positive towards the runway, and the z-axis positive vertically upwards. If the position of the aircraft in this coordinate system (the MLS coordinate frame) is (x_o, y_o, z_o), then the MLS signals have the values given by the formulas below.

$$R = \sqrt{x_o^2 + y_o^2 + z_o^2} \tag{135}$$

$$Az = \sin^{-1} \frac{-y_o}{R} \tag{136}$$

$$El = \tan^{-1} \frac{z_o}{\sqrt{(x_o - x_E)^2 + (y_o - y_E)^2}} \tag{137}$$

where x_E and y_E are the x and y coordinates of the elevation antenna phase center in the MLS coordinate frame.

The onboard sensors used are three body-mounted accelerometers, attitude gyros for the pitch, roll and yaw angles, attitude rate gyros, barometric altitude and sink rate, airspeed and radar altitude. The filter does not require expensive inertial platforms for sensor measurements. All of the onboard sensors are usually available on commercial aircraft except for the body accelerometers. However, the accelerometers are relatively inexpensive instruments and in many of the newer aircraft, a normal accelerometer already exists for pitch axis control. It should be noted that the radar altitude measurement is used in place of the MLS elevation signal only after the aircraft crosses the runway threshold since the aircraft flies out of the MLS elevation coverage during the flare maneuver.

To provide accurate estimates of the wind velocity components in the longitudinal, lateral and vertical directions, the filters were formulated using the aerodynamic properties of the aircraft. In addition, estimates of the bias errors in the three body-mounted accelerometers, barometric altitude and sink rate and attitude sensors are also obtained by the filters. The lateral filter uses the roll and yaw attitude, yaw rate and roll rate, the processed MLS y_o measurement, and the lateral accelerometer. The remaining measurements are used for the longitudinal filter. Discrete longitudinal and lateral Kalman filters were formulated with steady state gains, with some cross-coupling using second order terms and wind estimates.

The measurement bias terms were not included in the Kalman filter formulation and the steady state gain computations, but the required gain matrices were obtained using simple approximations. The basic form of the filters can be expressed by

$$\nu_k = y_k - C_x \hat{x}_k - C_w \hat{W}_k - C_b \hat{b}_k \quad , \tag{138}$$

$$\hat{x}_{k+1} = \phi \bar{x}_k + \Gamma u_k + \Gamma_w W_k + \psi \bar{\eta}_k \quad , \tag{139}$$

$$\hat{W}_{k+1} = \phi_w \bar{W}_k \quad , \tag{140}$$

$$\bar{x}_k = \hat{x}_k + F_x \nu_k \quad , \tag{141}$$

$$\bar{W}_k = \hat{W}_k + F_w \nu_k \quad , \tag{142}$$

$$\hat{b}_{k+1} = \hat{b}_k + F_b \nu_k \quad , \tag{143}$$

where $\hat{x}_k$, $\hat{W}_k$, $\hat{b}_k$ are predicted values and $\bar{x}_k$, $\bar{W}_k$, $\bar{\eta}_k$ are filtered values.

V. INITIAL SIMULATION RESULTS

As an initial evaluation of the basic approach used in the design of DIALS (i.e., a digital modern control structure tracking a trajectory defined on-line), and of the particular concepts used to obtain the various characteristics desired in each phase of the final approach and landing, the automatic landing system design and a six-degree-of-freedom non-linear aircraft model were simulated on a digital computer. The results of this initial evaluation are given in this section. A more detailed, realistic and in-depth evaluation, and further development of the automatic control law was performed prior to the flight testing of DIALS. The latter evaluation used an aircraft dynamics simulation validated by actual flight data for the TCV Research Aircraft, and realistic non-linear engine, actuator and servomechanism models [10]. The results of the detailed evaluation will be given together with the DIALS flight test results in a separate report.

The simulation used in the initial evaluation is a non-linear, six-degree-of-freedom, rigid aircraft model. The aerodynamic forces are generated using the stability derivatives of the Boeing 737-100 aircraft at an airspeed of 61.73 m/sec or 120 knots. The stability derivatives remain constant throughout the simulation; however, the dynamic pressure and the attitudes used in generating the aerodynamic forces and moments vary according to the path and wind conditions. Non-linear kinematic equations are used to generate the position of the center of mass and the attitude of the aircraft assuming a rigid structure. A detailed description of the aircraft equation of motion used in this simulation can be found in [20].

The servomechanisms and hydraulic actuators on the aircraft are modeled using first order dynamics by introducing an average lag in the control commands; however, non-linearities such as hysteresis or backlash are not included. The engine dynamics is modeled by a first order system whose time constant varies depending on whether the thrust is increasing or decreasing. The mechanical link from the aileron to the spoilers is modeled as an instantaneous, directly proportional motion as shown in (65).

Except for the engine dynamics, the overall actuator systems are assumed to be linear and contain no rate limits. However, it should be noted that all the DIALS control commands contain position or rate limits which are below the aircraft's actuator limits and capabilities. Thus, the lack of rate limits in the simulation does not introduce important errors in the results. However, non-linear actuator effects which are not considered part of this evaluation, but will be analyzed later.

The phases of flight considered in the simulation are the localizer and glideslope capture, the localizer and glideslope track, the crab/decrab maneuver, and flare until touchdown. Both the usual 3° glideslope and the steeper 4.5° glideslopes are simulated and the control performance evaluated in weather conditions that include gusts and steady winds. A simulation of the final approach that contains shear wind conditions for a steep approach (4.5° glidelsope) are also shown.

To evaluate the initial transient effects of the control law when it automatically engages the localizer and glideslope capture modes, the simulation is started prior to the engagement of DIALS. Thus, at the beginning of the simulation, the aircraft is in level flight, approaching the runway at the reference airspeed for landing (selected by the pilot) on a straight line which intercepts the runway centerline at a specified track

angle and corresponding yaw angle. For the simulation results shown in Figures 5 through 8, the aircraft is tracking a 30° intercept path to the runway centerline and flying a constant altitude path under the automatic control of a 3-D area navigation guidance and control mode.

This provides a realistic method of analyzing the initial transition effects, in comparison to starting the simulation at the instant DIALS engages, since it simulates the flight conditions more realistically. In particular, note that due to wind conditions and control errors, the aircraft does not always have exactly zero bank angle at localizer capture initiation, or exactly zero sink rate at glideslope capture initiation as can be seen in Figures 7, 8, and 9. Thus, transition effects can be analyzed more realistically.

It should be noted that similar transition effects are present as DIALS automatically engages each new control mode. Thus, transition from the localizer and glideslope capture modes to the corresponding track modes, followed by transition to the decrab and flare modes can cause undesirable transient effects, as in each case, control law changes such as some gain changes, introduction of integrators or changes in the commanded path, speed or attitude occur when each new mode is engaged. Observation of the simulations given in Figures 6 through 9 shows that such mode-to-mode transitions occur smoothly and without any undesirable transient effects in no wind as well as turbulent conditions. In fact, it would be difficult to determine the exact time the mode transitions occur from the plots shown. The smoothness of the mode-to-mode transitions was obtained using easy-on functions for gain changes, and special attention to the selection of the desired or commanded trajectory, as described in the section on flare. Smooth easy-on functions were not used when initiating or terminating integral feedback.

Figure 6 shows the simulation of a steep (4.5°) final approach and landing at a reference airspeed selection of 64.3 m/sec. or 125 knots in a no-wind condition and perfect measurements; i.e., no sensor error, noise or bias is present in this run. Thus, this run provides a baseline from which the effects of wind disturbances and measurement errors and noise can be analyzed and evaluated. These effects can be seen in the simulation shown in Figures 7 through 9 which contain both steady winds and gusts as well as measurement errors, noise and biases. In particular, Figure 9 shows the final approach and landing simulation in a wind shear condition.

The wind gust conditions are simulated according to the Dryden spectra. The models used for generating both the lateral and longitudinal wind gust velocities are given in Section II. The standard deviation of the wind gust velocities for the simulation runs shown here is .61 m/sec. or 2 ft/sec. in all three directions, with corresponding levels for moments due to gusts determined by the Dryden models. The steady winds are fixed relative to the earth coordinate axes. For the simulations shown in Figures 7 and 8, the steady wind is a 5.14 m/sec. or 10 knot quartering headwind. The shear wind conditions in Figure 9 simulate a steady headwind of 10 knots at altitudes above 200 feet. Between 200 feet and 100 feet, the headwind decreases at a rate of 4 knots per 100 feet. Below 100 feet, the headwind decreases at a rate of 8 knots per 100 feet. Thus, a 10 knot headwind at 200 feet changes to 2 knot tailwind at touchdown.

Depending on wind conditions, the localizer capture mode engages between 10 to 15 seconds after the start of the simulation. The exact time of the capture initiation is determined by the captive criterion given in (113). The baseline run in Figure 6 shows an initial inclination to roll away from the runway (as desired), reaching a maximum of about 8°

bank angle before settling at a level wings conditions. The cross-track error or distance from runway centerline has an overshoot of approximately 40 ft., and settles in approximately 50 sec. after capture initiation. The aircraft heading is similarly aligned with runway in about 55 sec. after the capture. The effects of the quartering headwind (corresponding to 7 knot cross-wind), as well as the effects of sensor noise and errors are seen to produce small deviations from the baseline response such as to increase the cross-track error overshoot to a maximum of about 75 ft. and to produce an initial tendency to roll towards the runway before reversing the roll direction due to initial errors in the estimates, and approximations used in developing the capture criterion.* However, the settling time is seen to be largely unaffected by wind conditions and remains in the vicinity of 50 seconds. In comparison to current ILS systems using inertial platforms and classical design structures, the overshoot performance shown here is of similar magnitude; however, the settling time required for DIALS is less than half the time required for these systems as can be seen in Figure 10 showing the response of a typical autoland system.

The glideslope capture mode is initiated between 22 to 27 seconds after the start of the simulation and vary shortly after the localizer capture mode is engaged. The variation in the capture initiation time is due to differing wind conditions and to different glideslopes. As can be seen from the pitch angle and sink rate behaviour prior to capture, the aircraft is not generally settled and trimmed on a constant altitude path when the glideslope capture mode engages. However, the capture mode

*Both the initial rolling tendency as well as the overshoots were considerably improved in futher development and will be shown in the flight test results.

produces an initial pitch down action in each case. Similarly, the sink rate is quickly reduced from its initial level to that required to follow the selected glideslope at the selected airspeed. It should be noted that there is practically no overshoot in the sink rate. The glideslope deviation similarly is reduced quickly. It should be noted that the aircraft is within 10 ft. of the glideslope within 15 seconds after the capture mode is engaged, and does not overshoot the glideslope. Finally, the capture of the steep (4.5°) glideslope is performed without any apparent difficulty. The effects of the wind conditions and sensor errors seem to produce minor deviations from the baseline run.

The localizer and glideslope track modes can be seen to provide the necessary control action to remain on the localizer and glideslope without any appreciable offset in different wind conditions. The type-1 property provided by the integral feedback appears satisfactory. It should also be noted that the deviations from the localizer and glideslope due to wind gusts tend to be small and are quickly corrected due to the gust alleviation or feedback of wind velocity estimates in the control law.

In all the simulation runs, the localizer capture mode is engaged first, followed by the glideslope capture within a few seconds. Thus, both capture maneuvers occur simultaneously, and settle on the desired path within 50 seconds. This simultaneous action and quick settling enables the capture maneuvers to start closer to the runway in the performance of close-in captures. The ability to use a shallow or steep glideslope according to termainal area conditions provides a further flexibility that can improve terminal area operations.

When a cross-wind is present, DIALS automatically crabs the aircraft into the wind while maintaining level wings, as desired. When the decrab

altitude is reached, DIALS performs a sideslip maneuver to align the aircraft heading with the runway. As can be seen in Figures 7 and 8, this is achieved by rolling the aircraft into the wind while reducing the heading relative to the runway.

The last control mode initiated is the flare maneuver. For the 3 and 4.5 degree glideslopes, the maneuver is initiated respectively at 31.2 meters (102.2 feet) and 40.8 meters (133.7 feet) of altitude. In all the simulation runs, the desired touchdown point is 396.2 meters (1300 feet) from the GPIP and the desired touchdown vertical velocity is .67 meters/ sec (-2.2 ft/sec) at 64.3 meters/ sec (125 knots) reference airspeed. For the -4.5° glideslope no wind no noise case the touchdown point and touchdown vertical velocity were respectively 381.9 meters (1253 feet) and -.88 meters/sec (-2.89 ft/sec).

For the cases of sensor noises and winds, the touchdown points and vertical velocities for the 4.5° glideslope with no shear, 3° glideslope with no shear, and 4.5° glideslope with shear are, respectively, 353.3 meters (1159 feet) and .79 meters/sec (-2.58 ft/sec), 377.7 meters (1239 feet) and .59 meters/sec (-1.93 ft/sec), and 436.8 meters (1433 feet) and .98 meters/sec (-3.29 ft/sec). For these cases the touchdown point is within 43.0 meters (141 feet) of the desired point. The highest touchdown sink rate, occuring for the shear wind case, exceeded the commanded sink rate by .30 m/sec (1 ft/sec). It should also be noted that in all the cases the touchdown pitch attitude is sufficiently positive to prevent premature nose wheel touchdown. The position offsets from runway centerline for these simulation runs were, respectively, .39 meters (1.27 feet), 1.22 meters (4.00 feet), .18 meters (.59 feet), and -.41 meters (-1.34 feet).

It is of interest to note that the wind shear is encountered while tracking a steep (4.5°) glideslope. As the wind velocity variation is simulated according to aircraft altitude, the time rate of change of the wind velocity is higher when flying a steeper glideslope. Thus, the effect of the wind shear on a 4.5° glideslope is 50% higher than on a 3° glideslope. Nevertheless, Figure 9 shows that the automatic landing system handles this wind shear scenario without any difficulty, and tracks the steep glideslope and flare path without introducing any extra altitude error.

VI. CONCLUSIONS

The design and development of a digital automatic landing system for a small commercial jet transport using modern digital control techniques has been considered. The system uses MLS position information, body-mounted accelerometers and on-board sensors usually available on commercial jets, but does not require costly inertial platforms. The phases of final approach to landing considered in the design were:

1) Localizer capture
2) Steep Gideslope capture
3) Localizer track
4) Steep Glideslope track
5) Decrab
6) Flare.

The simulation results presented indicate that the digital integrated automatic landing system can provide improved performance, without the use of inertial platforms, by providing 1) added flexibility in capturing and tracking steep glideslopes, 2) reducing the settling time to enable close-in captures, 3) reducing the sampling rate to 10 Hz to reduce computational requirements, 4) estimating wind velocities to provide better path control in wind shear conditions. The capability of flying a selectable steep glideslope, low overshoots and short settling times indicate a positive impact on airspace utilization, terminal area capacity in adverse weather conditions, perceived noise in airport communities, and avoidance of wake vortices.

The results have shown that the application of direct-digital-design and modern control theory methodologies can be used to engineer an

automatic landing system that performs the various lateral and longitudinal maneuvers with minimal gain changes using a fixed control law structure. To the author's knowledge, the digital integrated automatic landing system (DIALS) described in this report is the first automatic landing system designed using modern digital control methodologies whose performance has been demonstrated in successful flight tests.

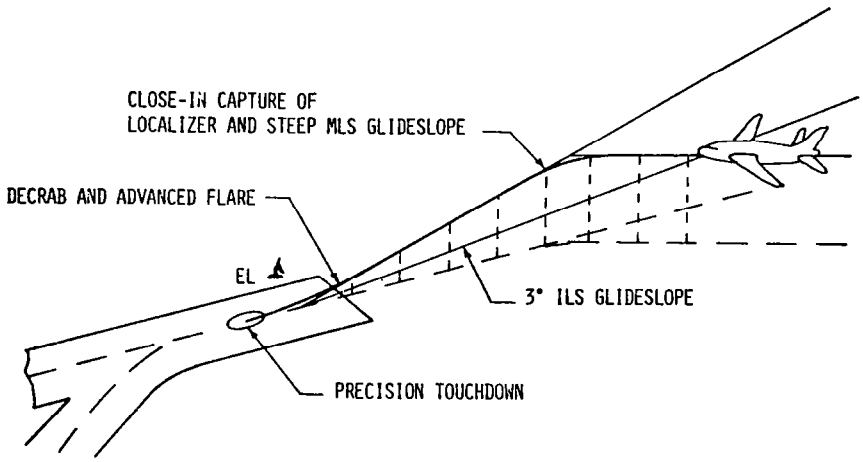

FIGURE 1 DIALS FLIGHT PATH GEOMETRY

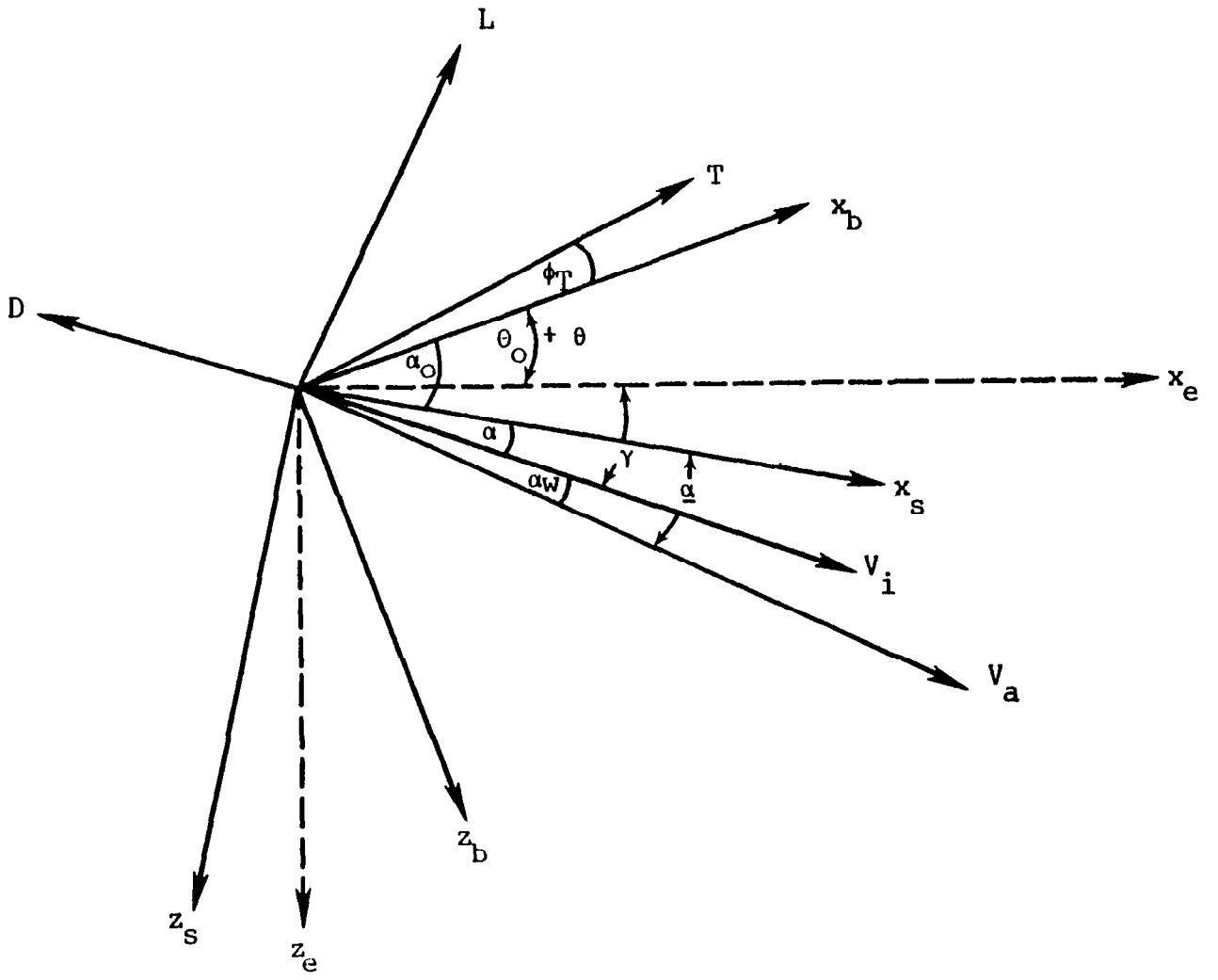

FIGURE 2 DEFINITION OF COORDINATE AXES, ANGLES AND FORCES.
(θ_o, θ, ϕ_T ARE MEASURED POSITIVE ccw, α_o, α_w, $\underline{\alpha}$, cw)

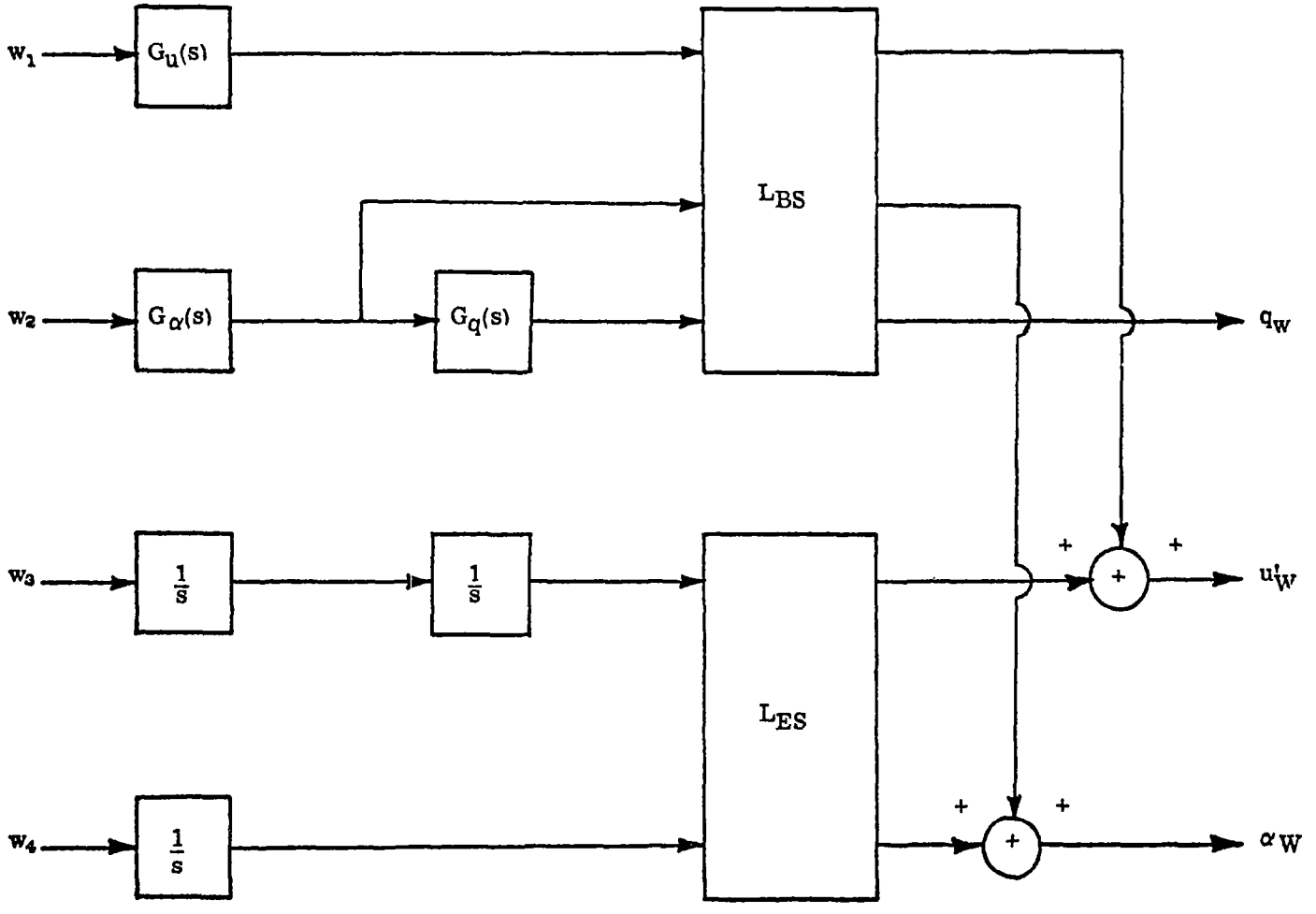

FIGURE 3 LONGITUDINAL WIND MODEL

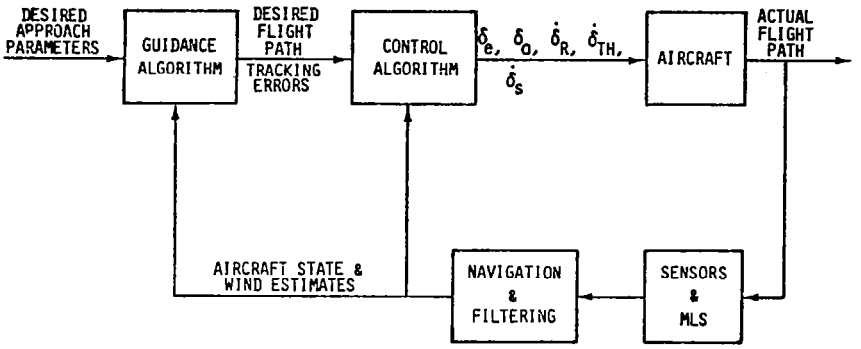

FIGURE 4 DIALS FUNCTIONAL BLOCK DIAGRAM

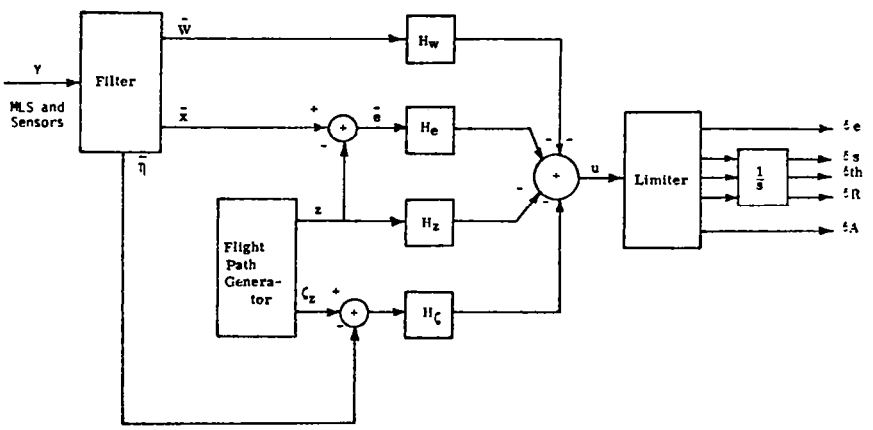

FIGURE 5 BLOCK DIAGRAM OF FEEDBACK LOOP

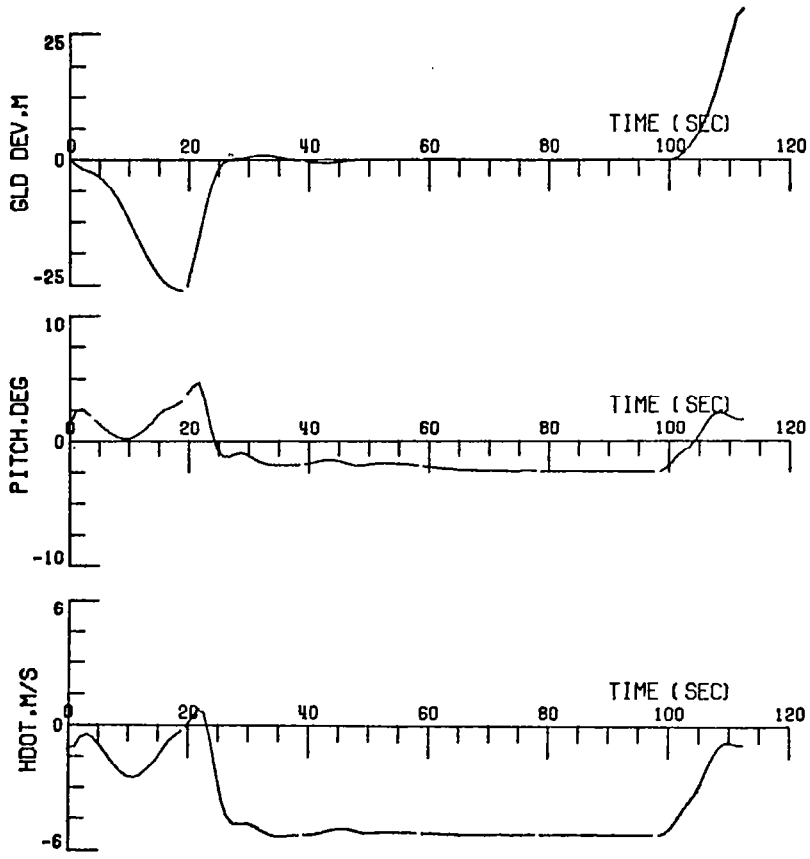

a. Longitudinal

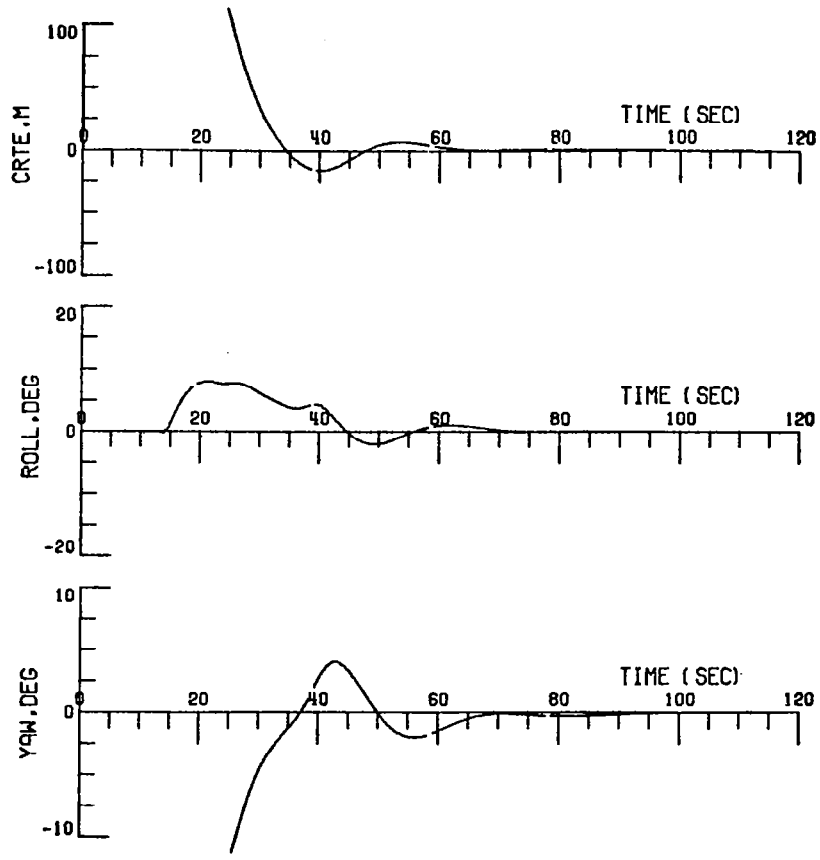

b. Lateral

FIGURE 6 4.5° GLIDESLOPE, 64.3 m/sec (125 knots), NO WINDS, NO SENSOR NOISE

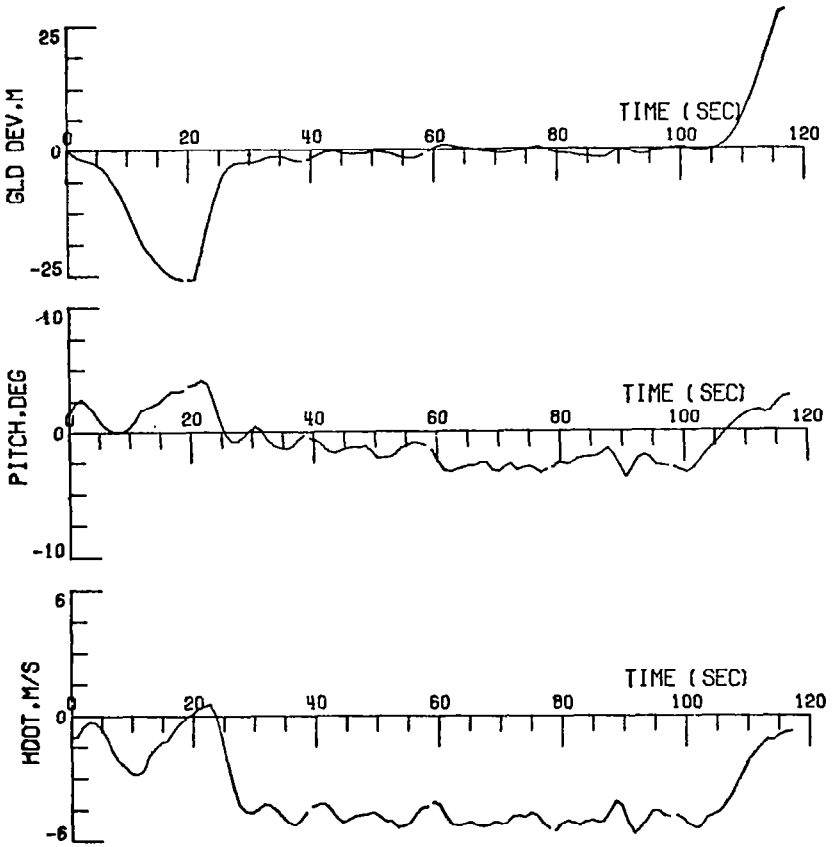

a. Longitudinal

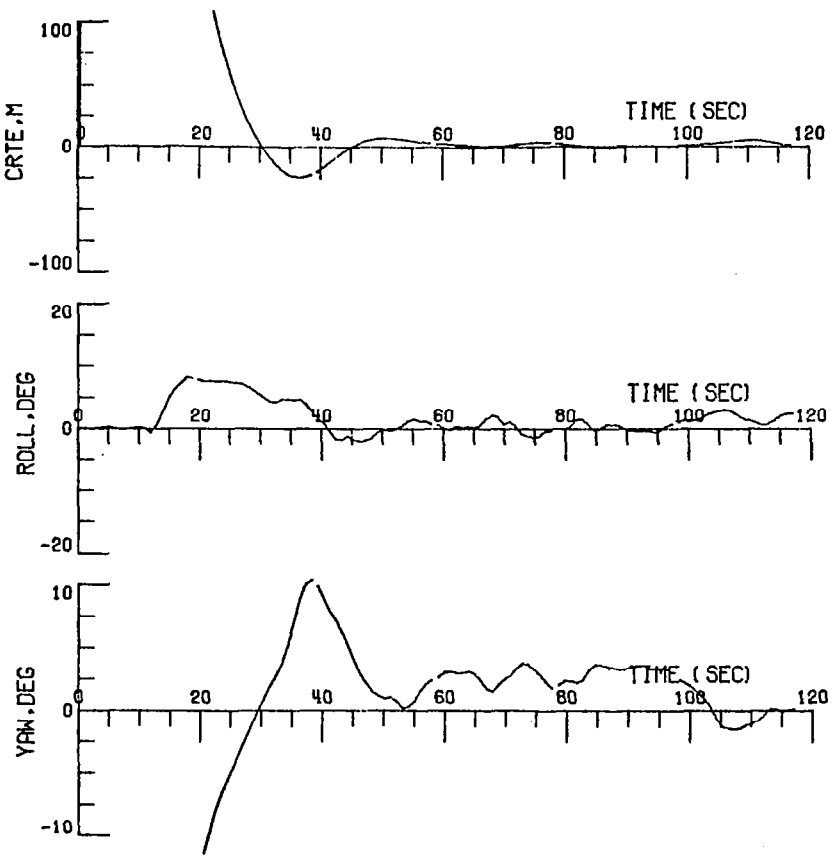

b. Lateral

FITURE 7 4.5° GLIDESLOPE, STEADY WINDS, GUSTS, SENSOR NOISES AND BIASES

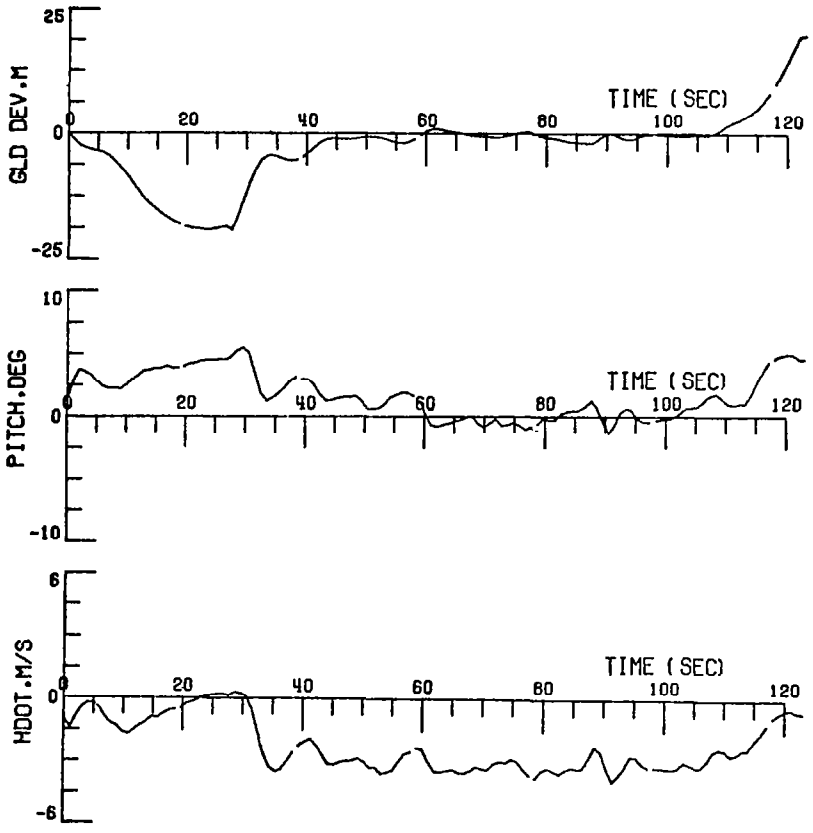

a. Longitudinal

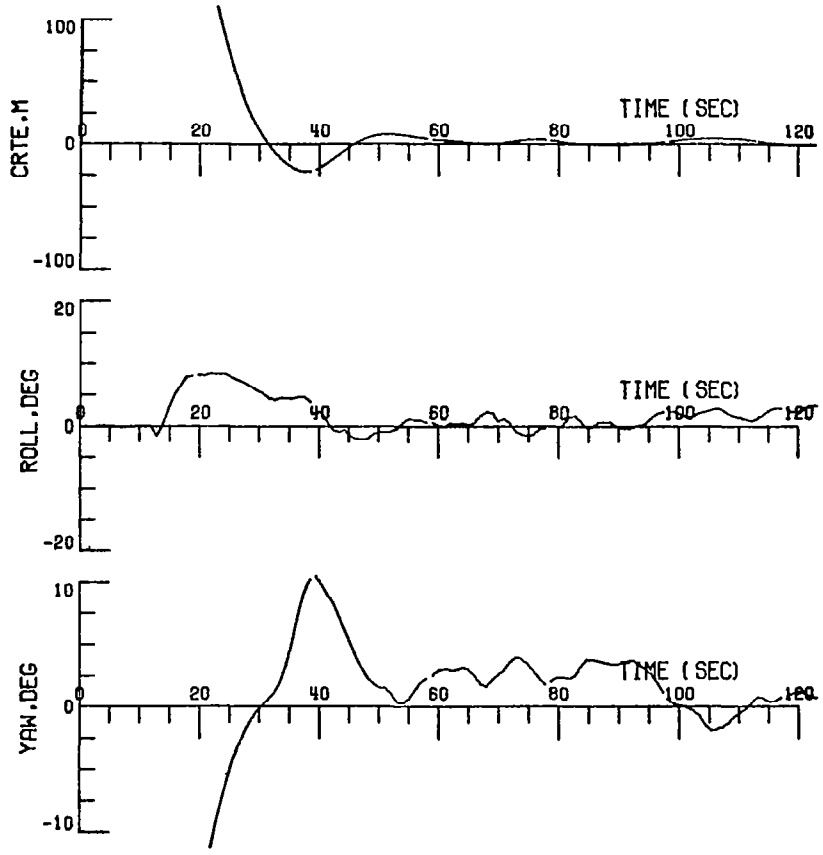

b. Lateral

FIGURE 8 3° GLIDESLOPE, 61.7 m/sec (120 knots), STEADY WINDS, GUSTS, SENSOR NOISES AND BIASES

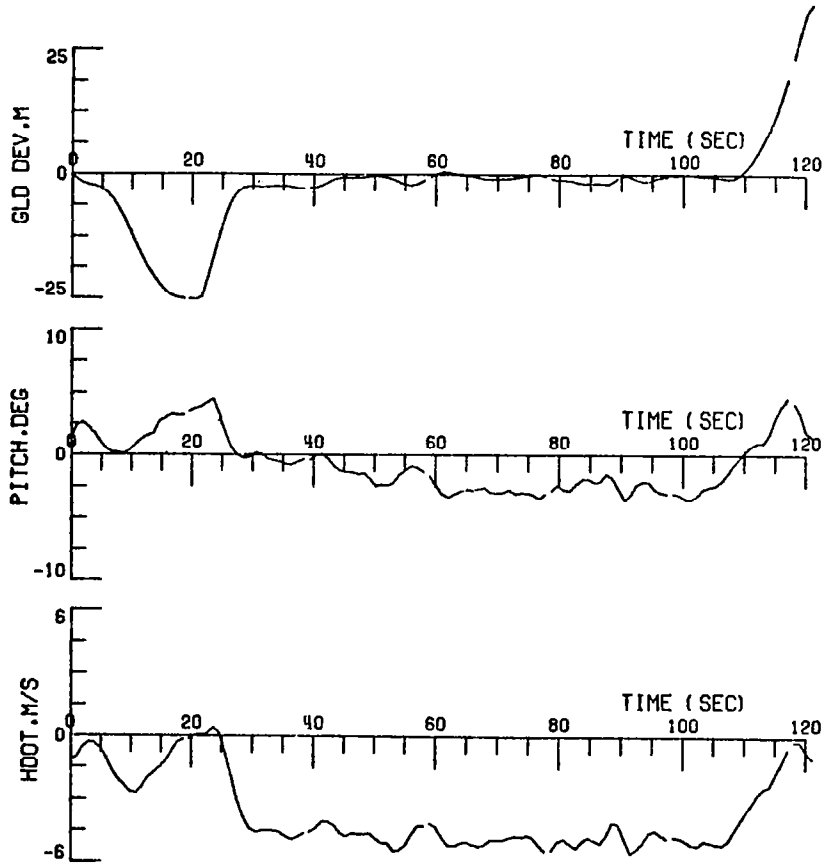

a. Longitudinal

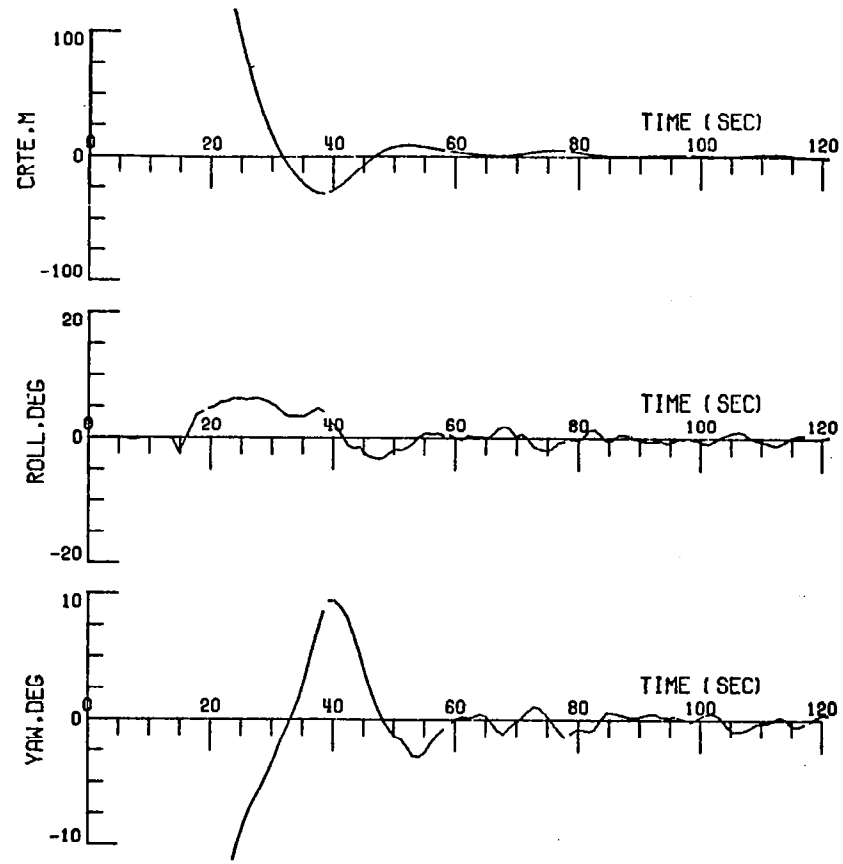

b. Lateral

FIGURE 9 4.5° GLIDESLOPE, STEADY WINDS, GUSTS, SHEAR WINDS, SENSOR NOISES AND BIASES

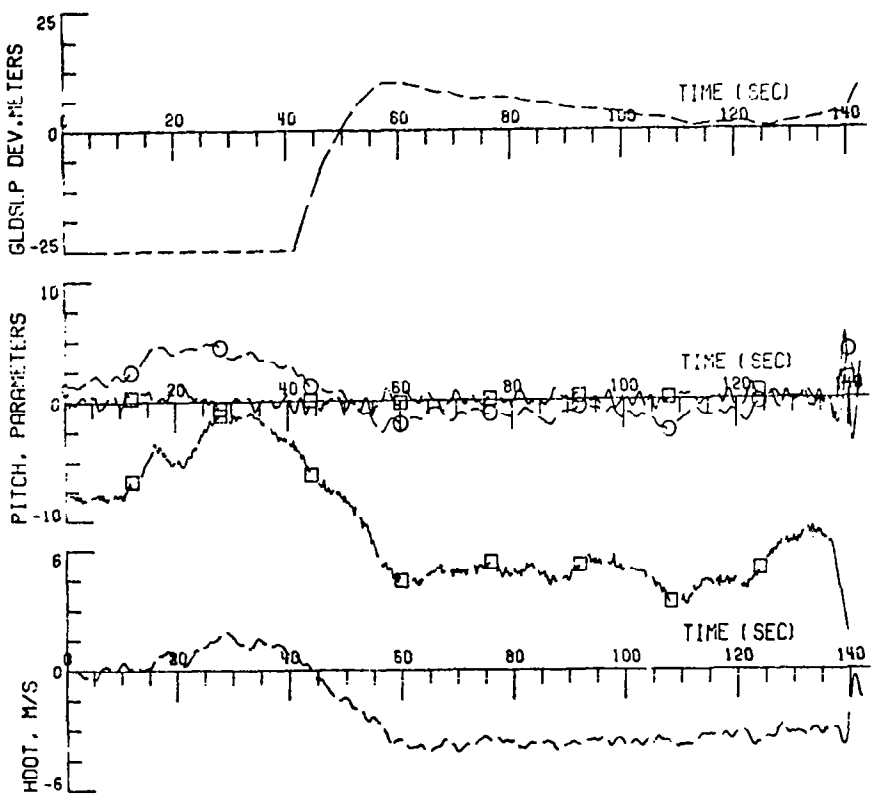

a. Longitudinal

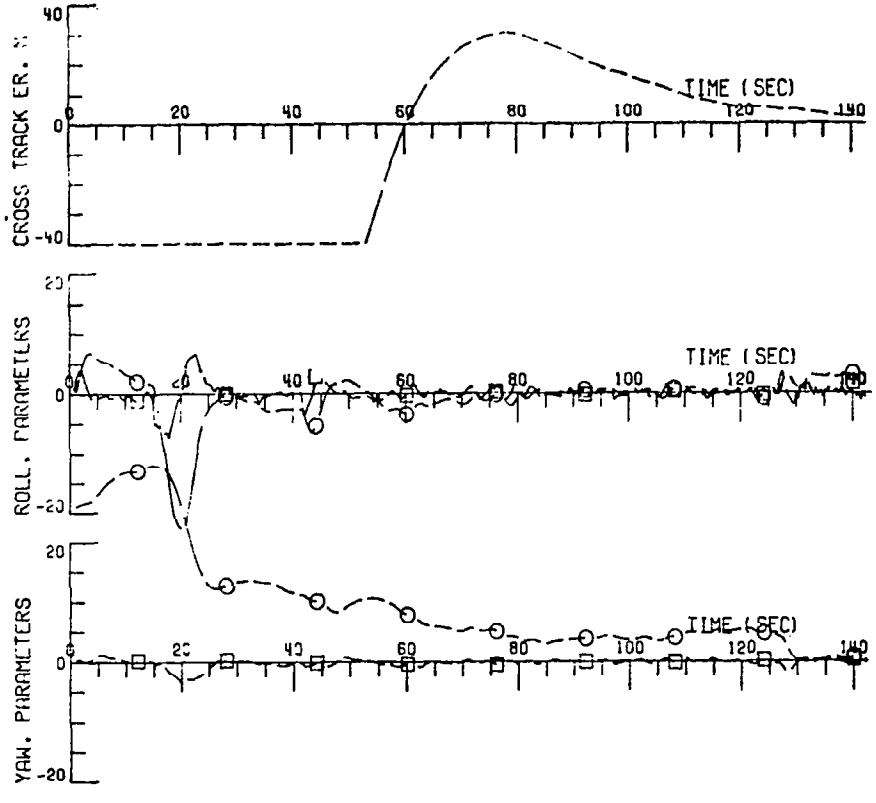

b. Lateral

FIGURE 10 RESPONSE OF AN INERTIALLY AUGMENTED ILS AUTOLAND SYSTEM 3° GLIDESLOPE, STEADY WINDS, GUSTS, SENSOR NOISES AND BIASES

VII. REFERENCES

1. Anon., "A New Guidance System for Approach and Landing," Vol. 2, Radio Technical Commission for Aeronautics, 1717 H Street N.W., Washington DC. Document DO-148, Dec. 18, 1970.

2. Reeder, J. P., R. T. Taylor, and T. M. Walsh, "New Designs and Operating Techniques for Improved Terminal Area Compatability," SAE, Air Transportation Meeting, Dallas, Texas, Apr. 30, 1974.

3. Halyo, N., "Development of an Optimal Automatic Control Law and Filter Algorithm for Steep Glideslope Capture and Glideslope Tracking," NASA CR-2720, Aug. 1976.

4. Halyo, N., "Development of a Digital Automatic Control Law for Steep Glideslope Capture and Flare," NASA CR-2834, June 1977.

5. Halyo, N., "Development of a Digital Guidance and Control Law for Steep Approach Automatic Landings Using Modern Control Techniques," NASA CR-3074, Feb. 1979.

6. Halyo, N., and Foulkes, R. E., "On the Quadratic Sampled-Data Regulator with Unstable Random Disturbances," IEEE SMC Cos. Proc., 1974 International Conf. on Syst., Man and Cybern., pp. 99 - 103, Oct. 1974.

7. Roskam, J., Flight Dynamics of Rigid and Elastic Airplanes, Parts I & II, Roskam Aviation and Engineering Corp., 519 Boulder, Lawrence, KS, 1972.

8. Etkin, B., Dynamics of Atmospheric Flight, John Wiley & Sons, Inc., New York, 1972.

9. McRuer, D., I. Ashkenas, and D. Graham, Aircraft Dynamics and Automatic Control, Princeton University Press, Princeton, NJ, 1973.

10. Halyo, N., and G. A. McAlpine, "Spectral Factorization of Random Processes with Multiplicity One," Proc. IEEE, Vol. 60, pp. 1006 - 1007, Aug. 1972.

11. Bode, H. W., and C. E. Shannon, "A Simplified Derivation of Linear Least-Squares Smoothing and Predicting Theory," Proc. IRE. Vol. 38, pp. 417 - 425, Apr. 1950.

12. Anderson, B. D. O., J. B. Moore, and S. B. Loo, "Spectral Factorization of Time Varying Covariance Functions," IEEE Trans. on Info. Theo., Vol. IT-15, pp. 550 - 557, Sept. 1959.

13. Halyo, N., and G. A. McAlpine, "On the Spectral Factorization of Non-Stationary Vector Random Processes," IEEE Trans. on Automatic Control, Vol. AC-19, No. 6., pp. 674 - 679.

14. Chalk, C. R., T. M. Harris, T. P. Neal, and E. F. Prichard, "Background Information and User Guide for MIL-F-8785B (ASG), 'Military Specification-Flying Qualities of Piloted Airplanes'," Air Force Flight Dynamics Report AFFDL-TR-69-72, Aug. 1969.

15. Kirk, D. E., Optimal Control Theory: An Introduction, Prentice Hall, Inc., Englewood Cliffs, NJ, 1970.

16. Halyo, N., and A. K. Caglayan, "A Separation Theorem for the Stochastic Sampled-Data LQG Problem," International J. of Control, Vol. 23, No. 2, pp. 237 - 244, Feb. 1976.

17. Kushner, H. J., Introduction to Stochastic Control, New York: Holt, Rinehart, and Winston, 1971.

18. Broussard, J. R., and M. J. O'Brien, "Feedforward Control to Track the Output of a Forced Model," IEEE Trans. on Automatic Control, Vol. AC-25, No. 4., pp. 851 - 854, Aug. 1980.

19. Halyo, N., and J. R. Broussard, "A Convergent Algorithm for the Stochastic Infinite-Time Discrete Optimal Output Feedback Problem," Proc. 1981 Joint Auto. Control Conference, Charlottesville, VA, June 1981.

20. Pines, S., S. F. Schmidt, F. Mann, "Automated Landing, Rollout and Turnoff Using MLS and Magnetic Cable Sensors," NASA CR-2907, October 1977.

1. Report No.	2. Government Accession No.	3. Recipient's Catalog No.
NASA CR-3681		

4. Title and Subtitle	5. Report Date
TERMINAL AREA AUTOMATIC NAVIGATION, GUIDANCE, AND CONTROL RESEARCH USING THE MICROWAVE LANDING SYSTEM (MLS) Part 5 - Design and Development of a Digital Integrated Automatic Landing System (DIALS) for Steep Final Approach Using Modern Control Techniques	April 1983
	6. Performing Organization Code

7. Author(s)	8. Performing Organization Report No.
Nesim Halyo	8242
	10. Work Unit No.

9. Performing Organization Name and Address	11. Contract or Grant No.
Analytical Mechanics Associates, Inc. 17 Research Road Hampton, VA 23666	NAS1-15116
	13. Type of Report and Period Covered
12. Sponsoring Agency Name and Address	Contractor Report
National Aeronautics and Space Administration Washington, DC 20546	14. Sponsoring Agency Code

15. Supplementary Notes

Langley Technical Monitor: Richard M. Hueschen
Final Report

16. Abstract

This report describes the design and development of a 3-D Digital Integrated Automatic Landing System (DIALS) for the Terminal Configured Vechicle (TCV) Research Aircraft, a B-737-100. The system was designed using sampled-data Linear-Quadratic-Gaussian (LQG) methods, resulting in a direct digital design with a modern control structure which consists of a Kalman filter followed by a control gain matrix, all operating at 10 Hz. DIALS uses Microwave Landing System (MLS) position, body-mounted accelerometers, as well as on-board sensors usually available on commercial aircraft, but does not use inertial platforms. The phases of the final approach considered are the localizer and glideslope capture which may be performed simultaneously, localizer and steep glideslope track or hold, crab/decrab and flare to touchdown. DIALS captures, tracks and flares from steep glideslopes ranging from 2.5° to 5.5°, selected prior to glideslope capture. To the author's knowledge, DIALS is the first modern control design automatic landing system successfully flight tested; the flight test results will be presented in a subsequent report. The results of an initial nonlinear simulation are presented here.

17. Key Words (Suggested by Author(s))	18. Distribution Statement
Automatic landing system, digital control, optimal control, direct digital design, steep final approach, localizer, glideslope, decrab, flare.	Unclassified-Unlimited Subject Category 08

19. Security Classif. (of this report)	20. Security Classif. (of this page)	21. No. of Pages	22. Price*
Unclassified	Unclassified	84	A05

For sale by the National Technical Information Service, Springfield, Virginia 22161

NASA-Langley, 1983